CHAPTER 3

# THERMOELASTIC DAMPING ANALYSIS IN MICRO AND NANOBEAM RESONATORS CONSIDERING MOORE-GIBSON-THOMPSON THERMOELASTICITY THEORY

## 3.1 Thermoelastic Damping Analysis in Microbeam Resonators Based on Moore–Gibson–Thompson Generalized Thermoelasticity Theory

### 3.1.1 Introduction[1]

This chapter is concerned with the study of thermoelastic damping (TED) in micro and nanobeam resonators considering the recently proposed Moore-Gibson-Thompson (MGT) thermoelasticity theory (Quintanilla, 2019). The chapter consists of three different subchapters that discusses three different problems. The first subchapter reveals the investigation of TED in microbeam based on the classical continuum theory in the framework of MGT thermoelastic equation. The second subchapter illustrates TED on the basis of modified couple stress theory (MCST) as nonclassical continuum theory in the context of MGT theory. The third subchapter focuses on the analysis of TED in

[1]The content of this subchapter is published in ***Acta Mechanica***, 231 (2020):3003-3015.

nanobeam resonators utilizing MGT equation and Eringen's nonlocal elasticity theory as the nonclassical continuum theory considering the effects of surface energy.

The current subchapter presents an analytical method for analyzing TED and dynamic behavior of microbeam resonators by formulating the problem on the basis of MGT generalized thermoelasticity theory. This work is carried out from the motivation by the previous articles as mentioned here. Ezzat et al. (2001) investigated TED and normal mode vibration in microbeam resonators and solved the coupled thermoelastic equations using the finite Fourier sine transform as well as Laplace transform methods. Sun et al. (2006) analyzed the static and dynamic behaviour of microbeam resonators in the context of generalized thermoelasticity theory with one relaxation time (LS model). To solve the coupled thermoelastic equations, they used the finite Fourier sine transform as well as Laplace transform methods and derived the expressions for deflection and thermal moment of the beam. In their work, it has also been reported that the deflection vibrates in a quasi-steady state mode while the thermal moment has a jump in the beginning and then vibrates in the same mode as deflection. Kakhki et al. (2016) analyzed TED and dynamic behavior of microbeam resonator utilizing thermoelasticity theory with one relaxation time. They adopted the Laplace transform technique for spatial variables to solve the coupled thermoelastic equations and established the expressions for deflection and thermal moment of the beam.

Being motivated from above work, this subchapter establishes the expressions of deflection and thermal moment for analyzing TED in microbeam resonators in the frame of the recently proposed heat conduction model, i.e., the MGT model. The finite Fourier sine transform and Laplace transform methods are used to solve the coupled thermoelastic equations. The vibration responses of deflection and thermal moment are analyzed in microbeams with simply supported and isothermal boundary conditions. The responses of deflection and thermal moment in beams are validated by comparing the results obtained under MGT model with the corresponding results under Lord-

Shulman (LS), and Green-Naghdi (GN-III) models. The obtained results show that the amplitudes of deflection and thermal moment are attenuated and the vibration frequency is increased due to the effect of thermoelastic coupling. It has been observed that the amplitudes of deflection under these three models are approximately the same while the amplitude of thermal moment under MGT model is higher than GN-III model and agrees with LS model. It has been further noticed that TED depends on the size of the beams when thermoelastic coupling effect is considered.

### 3.1.2 Governing equations

We consider the recently proposed Moore-Gibson-Thompson (MGT) thermoelasticity theory given by Quintanilla (2019) for analyzing TED and dynamic behavior of microbeam resonators. The heat conduction equation based on generalized MGT thermoelasticity theory for homogeneous and isotropic medium is given by

$$q\left(\boldsymbol{r},t\right)+\tau_q\dot{q}\left(r,t\right)=-\left[k\nabla T\left(\boldsymbol{r},t\right)+k^*\nabla\upsilon\left(\boldsymbol{r},t\right)\right] \tag{3.1.1}$$

The MGT thermoelasticity theory is the generalization of Lord-Shulman (LS) thermoelasticity theory and Green-Naghdi thermoelasticity theory of type III (GN-III). Hence, in particular the thermoelastic equation (3.1.1) yields:

**Case 1: Lord-Shulman (LS) model** if $k^*=0$, $\tau_q\neq 0$.

**Case 2: Green-Naghdi (GN-III) model** if $k^*\neq 0$, $\tau_q=0$.

By using Eqs. (2.1.8) and (3.1.1), we obtain the coupled heat conduction equation for a thermoelastic material as follows:

$$\left[k\nabla^2\dot{\theta}+k^*\nabla^2\theta\right]=\left(1+\tau_q\frac{\partial}{\partial t}\right)\left(\rho C_v\ddot{\theta}+T_0\beta\ddot{\epsilon}\right) \tag{3.1.2}$$

where $\beta=E\alpha_T/\left(1-2\nu\right)$.

### 3.1.3 Problem formulation

To analyze TED and dynamic behavior, we consider a thin microbeam resonator with rectangular cross-section of length $L$ $(0 \leq x \leq L)$, width $b$ $(-b/2 \leq y \leq +b/2)$, and thickness $h$ $(-h/2 \leq z \leq +h/2)$ as displayed in Figure 3.1.1. The both ends of the beam are simply supported and a uniform load $F$ of magnitude $F_0$ is initially applied on the upper surface of the beam which could express as the weight of the beam. We set the $x$-axis along the axis of the beam, $y$-axis along the beam width, and $z$-axis along the beam thickness. It is assumed that in equilibrium, the beam is unstrained, unstressed, and kept at reference temperature $T_0$ everywhere. Also, the upper and lower surfaces of the beam are adiabatic so that $\partial\theta/\partial z = 0$ at $z = \pm h/2$.

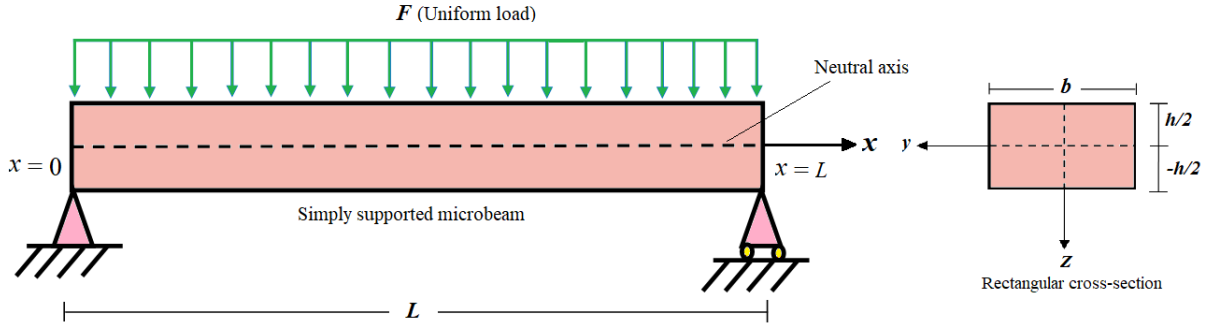


Figure 3.1.1: Simply supported microbeam subjected to a uniform load initially applied on the upper surface of the beam.

According to the dimensions of the beam, the usual Euler-Bernoulli beam theory is assumed to be reasonable. Therefore, based on Euler-Bernoulli beam assumptions, the displacement functions can be defined as follows:

$$u_x = -z\frac{\partial w}{\partial x},\ u_y = 0,\ u_z\left(x, y, z, t\right) = w\left(x, t\right) \tag{3.1.3}$$

where $t$ denotes the time and $w$ denotes the deflection of the beam. The one-dimensional

constitutive equation is given by

$$\sigma_{xx} = -Ez\frac{\partial^2 w}{\partial x^2} - \beta\theta \tag{3.1.4}$$

The flexural moment of the cross-section of the beam is given by

$$M(x,t) = -\int_{-\frac{h}{2}}^{+\frac{h}{2}} b\sigma_{xx} z dz = EI\frac{\partial^2 w}{\partial x^2} + M_T \tag{3.1.5}$$

where $I = bh^3/12$ represents the moment of inertia and the thermal moment $M_T$ from Eq. (2.1.3) further can be expressed by

$$M_T = b\beta\int_{-\frac{h}{2}}^{+\frac{h}{2}} \theta z dz \tag{3.1.6}$$

The equation of transverse motion of the beam is

$$\frac{\partial^2 M}{\partial x^2} + \rho A\frac{\partial^2 w}{\partial t^2} = 0 \tag{3.1.7}$$

Substituting the value of $M$ from Eq. (3.1.5) into Eq. (3.1.7), the equation of motion for the beam can be derived as:

$$EI\frac{\partial^4 w}{\partial x^4} + \frac{\partial^2 M_T}{\partial x^2} + \rho A\frac{\partial^2 w}{\partial t^2} = 0 \tag{3.1.8}$$

Substituting Eq. (3.1.3) into Eq. (2.1.3), the coupled heat conduction equations yields

$$\left[k\frac{\partial}{\partial t} + k^*\right]\left(\frac{\partial^2\theta}{\partial x^2} + \frac{\partial^2\theta}{\partial z^2}\right) = \left(1 + \tau_q\frac{\partial}{\partial t}\right)\left(\rho C_v\ddot{\theta} - T_0\beta z\frac{\partial^4 w}{\partial x^2\partial t^2}\right) \tag{3.1.9}$$

Multiplying Eq. (3.1.9) both sides by $b\beta z$ and integrating with respect to $z$ in the range

from $-h/2$ to $+h/2$, we have

$$\left[k\frac{\partial}{\partial t}+k^*\right]\left(\frac{\partial^2 M_T}{\partial x^2}+b\beta\int_{-\frac{h}{2}}^{+\frac{h}{2}} z\frac{\partial^2\theta}{\partial z^2}dz\right)=\left(1+\tau_q\frac{\partial}{\partial t}\right)\left(\rho C_v\frac{\partial^2 M_T}{\partial t^2}-T_0\beta^2 I\frac{\partial^4 w}{\partial x^2\partial t^2}\right) \tag{3.1.10}$$

When the beam is very thin, it can be assumed that the temperature increment changes along the thickness direction in terms of $sin\,(Pz)$ function in which $P=\pi/h$ (Sun et al., 2006). From Eq. (3.1.6), the thermal moment $M_T$ can further be written as:

$$M_T=-\frac{1}{P^2}\int_{-\frac{h}{2}}^{+\frac{h}{2}} b\beta\frac{\partial^2\theta}{\partial z^2}zdz \tag{3.1.11}$$

Inserting Eq. (3.1.11) into Eq. (3.1.10), one can obtain

$$\left[k\frac{\partial}{\partial t}+k^*\right]\left(\frac{\partial^2}{\partial x^2}-P^2\right)M_T-\left(1+\tau_q\frac{\partial}{\partial t}\right)\left(\rho C_v\frac{\partial^2 M_T}{\partial t^2}-T_0\beta^2 I\frac{\partial^4 w}{\partial x^2\partial t^2}\right)=0 \tag{3.1.12}$$

For convenience, we use some non-dimensional form of variables as follows:

$$\zeta=\frac{x}{L},\ \phi=\frac{w}{h},\ \tau=\frac{t\varepsilon}{L},\ \varepsilon=\sqrt{\frac{E}{\rho}},\ \psi=\frac{M_T}{EAh},\ \tau_1=\frac{\tau_q\varepsilon}{L} \tag{3.1.13}$$

where $\phi$ and $\psi$ are the non-dimensional deflection and non-dimensional thermal moment of the microbeam resonator, respectively. Substituting Eq. (3.1.13) into Eqs. (3.1.8) and (3.1.12), the dimensionless form of coupled governing equations can be derived as follows:

$$\frac{\partial^2\psi}{\partial\xi^2}+M_1\frac{\partial^4\phi}{\partial\xi^4}+\frac{\partial^2\phi}{\partial\tau^2}=0 \tag{3.1.14}$$

$$\left[k_0'+\frac{\partial}{\partial\tau}\right]\left(\frac{\partial^2\psi}{\partial\zeta^2}-M_2\psi\right)-\left(1+\tau_1\frac{\partial}{\partial\tau}\right)\left(M_3\frac{\partial^2\psi}{\partial\tau^2}-M_4\frac{\partial^4\phi}{\partial\zeta^2\partial\tau^2}\right)=0 \tag{3.1.15}$$

where $M_1=\frac{h^2}{12L^2}$, $M_2=P^2L^2$, $M_3=\frac{\rho C_v L}{k}$, $M_4=\frac{T_0\beta^2h^2\varepsilon}{12LkE}$, $k_0'=\frac{k^*L}{k\varepsilon}$.

If we ignore the thermoelastic coupling effects from Eqs. (3.1.8) and (3.1.12), then the governing equations of uncoupled system and the equation of motion of microbeam

resonator can be reduced to the forms as

$$\begin{cases} EI\frac{\partial^4 w}{\partial x^4} + \rho A\frac{\partial^2 w}{\partial t^2} = 0 \\ \left[k\frac{\partial}{\partial t} + k^*\right]\left(\frac{\partial^2\theta}{\partial x^2} + \frac{\partial^2\theta}{\partial z^2}\right) = \left(1 + \tau_q\frac{\partial}{\partial t}\right)\left(\rho C_v\frac{\partial^2\theta}{\partial t^2}\right) \end{cases} \tag{3.1.16}$$

### 3.1.4 Initial and boundary conditions

Let us now consider the boundary as well as initial conditions and make attempt to solve the problem. Firstly, we suppose a uniform load $F$ of magnitude $F_0$ is initially applied on the upper surface of the beam resonator. Therefore, the initial conditions can be set in the following form

$$\begin{cases} \phi|_{\tau=0} = F_0\left(\zeta - 2\zeta^2 + \zeta^4\right) \\ \frac{\partial\phi}{\partial\tau}|_{\tau=0} = \frac{\partial^2\phi}{\partial\tau^2}|_{\tau=0} = 0 \\ \psi|_{\tau=0} = 0 \\ \frac{\partial\psi}{\partial\tau}|_{\tau=0} = \frac{\partial^2\psi}{\partial\tau^2}|_{\tau=0} = 0 \end{cases} \tag{3.1.17}$$

Also, we consider the case when the ends of the beam are simply supported, therefore, the boundary conditions take the form

$$\begin{cases} \phi|_{\zeta=0} = \phi|_{\zeta=1} = 0 \\ \frac{\partial^2\phi}{\partial\zeta^2}|_{\zeta=0} = \frac{\partial^2\phi}{\partial\zeta^2}|_{\zeta=1} = 0 \\ \psi|_{\zeta=0} = \psi|_{\zeta=1} = 0 \end{cases} \tag{3.1.18}$$

### 3.1.5 Solution of the problem

In this part, we use a finite Fourier sine transform and Laplace transform methods to solve the coupled heat conduction equations (3.1.14) and (3.1.15) of the microbeam.

Applying finite Fourier sine transform both sides of Eqs. (3.1.14) and (3.1.15) and using Eq. (3.1.18), we have

$$\frac{\partial^2 \phi_m}{\partial \tau^2} + M_1 r_m^4 \phi_m - r_m^2 \psi_m = 0 \tag{3.1.19}$$

$$\left[k_0' + \frac{\partial}{\partial \tau}\right]\left(r_m^2 \psi_m + M_2 \psi_m\right) + \left(1 + \tau_1 \frac{\partial}{\partial \tau}\right)\left(M_3 \frac{\partial^2 \psi_m}{\partial \tau^2} + M_4 r_m^2 \frac{\partial^2 \phi_m}{\partial \tau^2}\right) = 0 \tag{3.1.20}$$

and the corresponding initial conditions take the form

$$\begin{cases} \phi_m|_{\tau=0} = \frac{48}{r_m^5} F_0 \\ \frac{\partial \phi_m}{\partial \tau}|_{\tau=0} = \frac{\partial^2 \phi_m}{\partial \tau^2}|_{\tau=0} = 0 \\ \psi_m|_{\tau=0} = 0 \\ \frac{\partial \psi_m}{\partial \tau}|_{\tau=0} = \frac{\partial^2 \psi_m}{\partial \tau}|_{\tau=0} = 0 \end{cases} \tag{3.1.21}$$

where $r_m = m\pi$, $m = 1,\ 3,\ 5\,, ....$

In above equations, $\phi_m$ and $\psi_m$ denote the Fourier transform of $\phi$ and $\psi$, respectively. Applying Laplace transform to both sides of Eqs. (3.1.19) and (3.1.20), the new governing equations in view of Eq. (3.1.21) become

$$s^2 \overline{\phi}_m - s\frac{48}{r_m^5} F_0 + M_1 r_m^4 \overline{\phi}_m - r_m^2 \overline{\psi}_m = 0 \tag{3.1.22}$$

$$\begin{aligned} &\left[\left(k_0' + s\right)\left(r_m^2 + M_2\right) + M_3 s^2 + \tau_1 M_3 s^3\right] \overline{\psi}_m \\ &\qquad + M_4 r_m^2 \left(s^2 + \tau_1 s^3\right) \overline{\phi}_m = \frac{48}{r_m^3} F_0 \left(1 + \tau_1\right) M_4 \end{aligned} \tag{3.1.23}$$

where $\overline{\phi}_m$ and $\overline{\psi}_m$ represent the Laplace transform of $\phi_m$ and $\psi_m$, respectively. From Eqs. (3.1.22) and (3.1.23), one can obtain

$$\overline{\phi}_m = \frac{48}{r_m^5} F_0 \left[\frac{g_0 + g_1 s + g_2 s^2 + g_3 s^3 + g_4 s^4}{\overline{g}_0 + \overline{g}_1 s + \overline{g}_2 s^2 + \overline{g}_3 s^3 + \overline{g}_4 s^4 + \overline{g}_5 s^5}\right] \tag{3.1.24}$$

where $\overline{g}_0 = k_0' \left(r_m^2 + M_2\right) M_1 r_m^4$, $\overline{g}_1 = \left(r_m^2 + M_2\right) M_1 r_m^4$, $\overline{g}_2 = k_0' \left(r_m^2 + M_2\right) + \left(M_1 M_3 + M_4\right) r_m^4$, $\overline{g}_3 = \left(r_m^2 + M_2\right) + \left(M_1 M_3 + M_4\right) \tau_1 r_m^4$, $\overline{g}_4 = M_3$, $\overline{g}_5 = \tau_1 M_3$, $g_0 = \left(1 + \tau_1\right) M_4 r_m^4$, $g_1 = k_0' \left(r_m^2 + M_2\right)$, $g_2 = \left(r_m^2 + M_2\right)$, $g_3 = M_3$, $g_4 = \tau_1 M_3$.

After using the inversion of Laplace transform of Eq. (3.1.24), we get the solution for deflection function $\Phi_m$ as follows:

$$\phi_m \left(m, \tau\right) = \frac{48 F_0}{r_m^5} \sum_{\alpha} \frac{\left(g_0 + g_1 \alpha + g_2 \alpha^2 + g_3 \alpha^3 + g_4 \alpha^4\right) e^{\alpha \tau}}{\left(\overline{g}_1 + 2\overline{g}_2 \alpha + 3\overline{g}_3 \alpha^2 + 4\overline{g}_4 \alpha^3 + 5\overline{g}_5 \alpha^4\right)} \tag{3.1.25}$$

where $\alpha$ is the all five roots of the equation $\overline{g}_0 + \overline{g}_1 \alpha + \overline{g}_2 \alpha^2 + \overline{g}_3 \alpha^3 + \overline{g}_4 \alpha^4 + \overline{g}_5 \alpha^5 = 0$. Now, the deflection function can be obtained by the following relation

$$\phi \left(m, \tau\right) = 2 \sum_{m=1,\,3,\ldots.}^{\infty} \phi_m \left(m, \tau\right) sin \left(r_m \zeta\right) \tag{3.1.26}$$

Substituting Eq. (3.1.25) into Eq. (3.1.26), we arrive at the final expression for the non-dimensional deflection of the microbeam resonator in the form

$$\phi \left(m, \tau\right) = 96 F_0 \sum_{m=1,\,3,\ldots.}^{\infty} \frac{1}{r_m^5} \sum_{\alpha} \frac{\left(g_0 + g_1 \alpha + g_2 \alpha^2 + g_3 \alpha^3 + g_4 \alpha^4\right) e^{\alpha \tau}}{\left(\overline{g}_1 + 2\overline{g}_2 \alpha + 3\overline{g}_3 \alpha^2 + 4\overline{g}_4 \alpha^3 + 5\overline{g}_5 \alpha^4\right)} sin \left(r_m \zeta\right) \tag{3.1.27}$$

In a similar way, the non-dimensional thermal moment $\psi \left(m, \tau\right)$ can be derived as:

$$\psi \left(m, \tau\right) = 96 F_0 \sum_{m=1,\,3,\ldots.}^{\infty} \frac{1}{r_m^5} \sum_{\alpha} \frac{\left(e_0 + \alpha + e_1 \alpha^2\right) e^{\alpha \tau}}{\left(\overline{g}_1 + 2\overline{g}_2 \alpha + 3\overline{g}_3 \alpha^2 + 4\overline{g}_4 \alpha^3 + 5\overline{g}_5 \alpha^4\right)} sin \left(r_m \zeta\right) \tag{3.1.28}$$

where $e_0 = \left(1 + \tau_1\right) M_1 M_4 r_m^6$, $e_1 = \left(1 + \tau_1\right) A_4 r_m^4$.

Further, if the thermoelastic coupling effect is ignored then in view of Eq. (3.1.16), the dimensionless deflection $\left(\phi_0 \left(m, \tau\right)\right)$ under uncoupled case can be derived in a similar way.

### 3.1.6 Numerical results and discussion

In this section, the analytical results are illustrated and the nature of dimensionless deflection and dimensionless thermal moment of microbeam resonator initially subjected to a uniform load is investigated. The beam is assumed to be made of Silicon material. We aim to analyze the effects of various beam parameters such as length, thickness, applied load, and phase-lags on dimensionless deflection and dimensionless thermal moment at different time of vibration of the beam. The effects of thermoelastic coupling on TED are also demonstrated in the present context. Here, we compare the obtained results of MGT model to the existing results under LS model (as given by Sun et al. (2006)) and GN-III model. There is a lack of the value of the thermal conductivity rate $k^*$ associated in the heat conduction equation, therefore, we also consider here three different cases for dimensionless parameter $k_0'$ to see the effect of $k^*$ i.e. $k_0' \ll 1$, $k_0' = 1$, and $k_0' \gg 1$. For numerical results, the considered values of the Silicon material are given below (Duwel et al., 2003):

$\rho = 2330\, Kg/m^3$, $E = 169\, GPa$, $\nu = 0.22$, $k = 156\, Wm^{-1}K^{-1}$, $\alpha_T = 2.59 \times 10^{-6} K^{-1}$, $C_v = 713\, JKg^{-1}K^{-1}$, $T_0 = 293\, K$.

The microbeam aspect ratios are fixed here as $L/h = 10$ and $b/h = 0.5$ except where its effect is shown. It is clear that when the thickness $h$ varies, the length $L$ and width $b$ change simultaneously with $h$. The thickness is fixed as the aspect ratio, $h/h_0 = 0.5$ where $h_0 = 20\, \mu m$ excluding Figure 3.1.9. The graphs are plotted for first vibration mode i.e. $m = 1$. Figures 3.1.2-3.1.4 and 3.1.7-3.1.12 are plotted for the case when $k_0' \ll 1$. Figures 3.1.5 and 3.1.6 show the effects of $k_0'$ on variation of deflection and thermal moment. Note that the considered value of phase-lag time in dimensionless form is $\tau_1 = 1.9$.

Fig. 3.1.2 shows the variation of the amplitude of the dimensionless deflection of the microbeam resonator with respect to the dimensionless time for MGT, LS, and GN-III models. It has been observed that the nature of the vibrations of the deflection

is approximately the same for all the three models.

Fig. 3.1.3 demonstrates the deflection difference between $\phi_0$ (deflection under uncoupled system) and $\phi$ (deflection under coupled system for MGT, LS, and GN-III models) to see the decay due to TED and coupling effects of the amplitude of the vibration with respect to the time. It can be concluded that when time increases, the amplitude of the $\phi_0 - \phi$ increases rapidly. This shows that the amplitude of $\phi$ decreases and hence, the mechanical energy of the microbeam resonator is dissipated. The coupling effect under MGT and LS models are the same. However, a disagreement in results of these two models with GN-III model can be noted fro the figure. It is observed that the MGT and LS models predict less energy dissipation of deflection as compared to GN-III model.

The time variation of amplitude of thermal moment at the middle point of the beam under MGT, LS, and GN-III models is shown in Fig. 3.1.4. It can be observed that the dissipation of the amplitude of the thermal moment is significant with time. In the beginning, the amplitude of the thermal moment has a jump and then starts to oscillate quickly in a quasi-steady state mode. A similar fact has been reported by Sun et al. (2006) for the case of thermoelasticity theory with one relaxation parameter (LS model). Also, the response of vibration of the thermal moment under MGT and LS models is the same and higher than GN-III model. MGT and LS models show highest numerical value of thermal moment, the GN-III model showing the smallest value in absolute.

Figs. 3.1.5 and 3.1.6 depict the variations of deflection and thermal moment, respectively, for varying dimensionless parameter $k_0'$ ($k_0' \gg 1$, $k_0' = 1$, $k_0' \ll 1$) and show the effect of thermal conductivity rate $k^*$ of the material associated in the present non-Fourier heat conduction equation. One can observe that there is a significant effect of this parameter on variations of deflection and thermal moment. We particularly note that when $k_0' \gg 1$ or $k_0' = 1$, there is jump in the amplitude of deflection when dimensionless time ($\tau$) is greater than 60. In this case, the vibration response of amplitude of

deflection is more faster, therefore, the dissipation of energy in beam resonator is more quickly. Hence, to minimize the energy dissipation, the value of thermal conductivity $k^*$ can be chosen such that $k_0' \ll 1$. Also, when $k_0' \gg 1$ or $k_0' = 1$, there is jump of the amplitude of thermal moment in the starting and then, it starts to oscillate in the quasi-steady state mode.

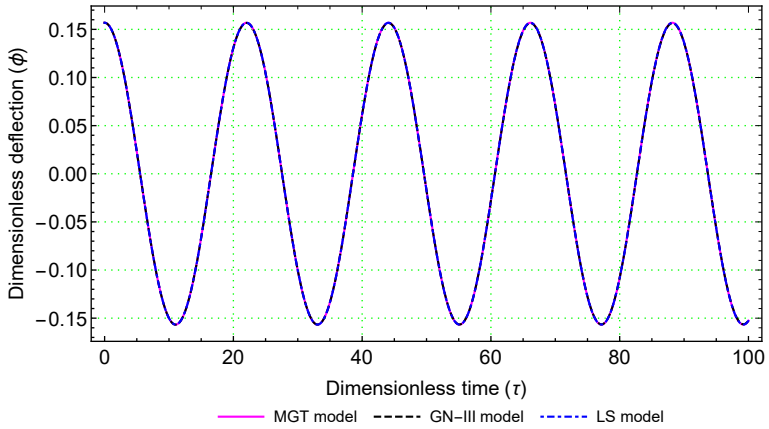


Figure 3.1.2: Variation of dimensionless deflection with respect to the dimensionless time for middle point of the beam.

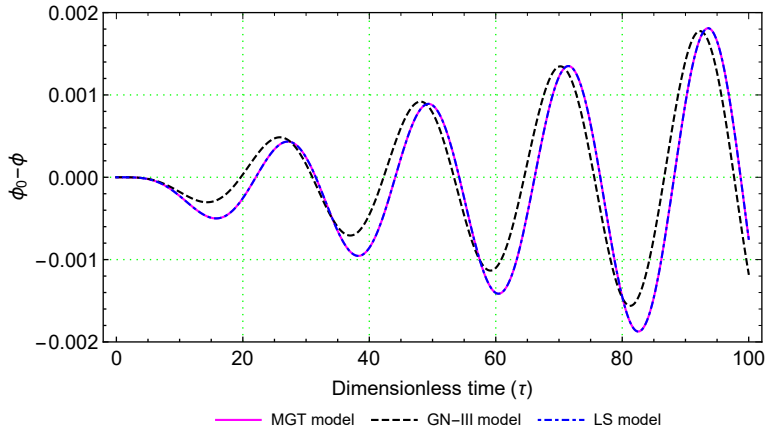


Figure 3.1.3: Variation of the deflection difference $(\phi_0 - \phi)$ with respect to the dimensionless time for middle point of the beam.

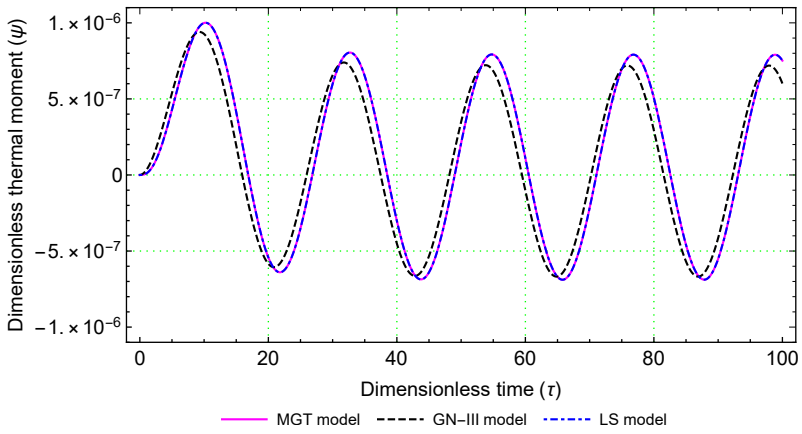


Figure 3.1.4: Variation of the dimensionless thermal moment with respect to the dimensionless time for the middle point of the beam.

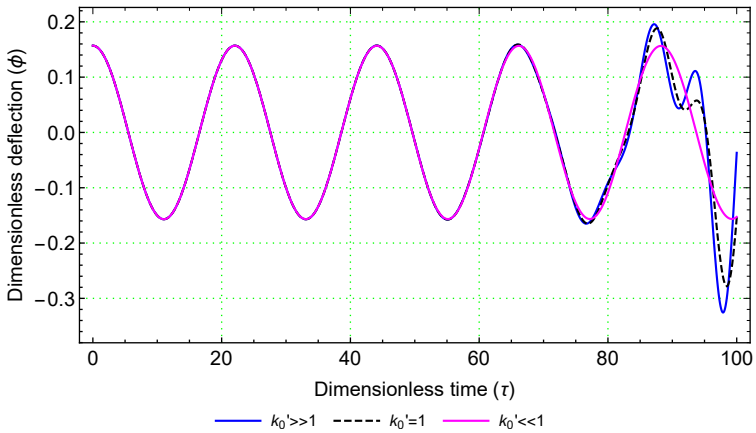


Figure 3.1.5: Variation of the dimensionless deflection with respect to dimensionless time for varying dimensionless parameter $k_0'$ ($k_0' \gg 1$, $k_0' = 1$, $k_0' \ll 1$).

Fig. 3.1.7 represents the vibration response of deflection with respect to time for different values of the applied load on the upper surface of the beam for the case of MGT model. For this, we consider the case when the magnitudes of the applied load are $F_0 = 1$, $F_0 = 2$, and $F_0 = 3$. Here, we observe that the effects of applied load on vibration response of deflection of the beam is very much prominent. It is clear that

the amplitude of the deflection increases by increasing the values of the applied load as it was expected.

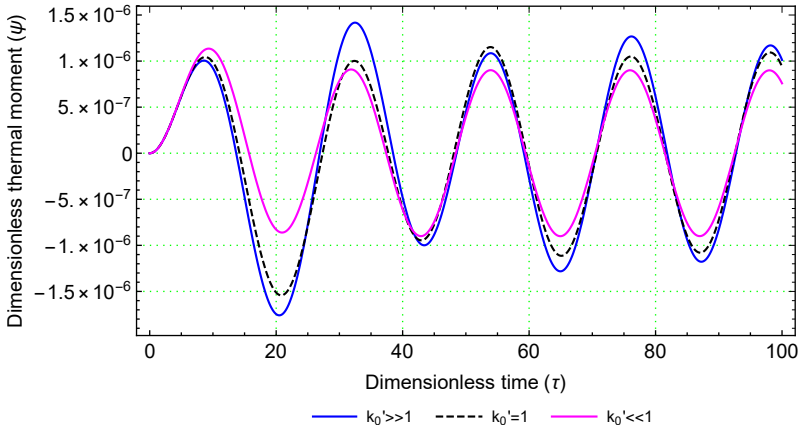


Figure 3.1.6: Variation of the dimensionless thermal moment with respect to dimensionless time for varying dimensionless parameter $k_0'$ ($k_0' \gg 1$, $k_0' = 1$, $k_0' \ll 1$).

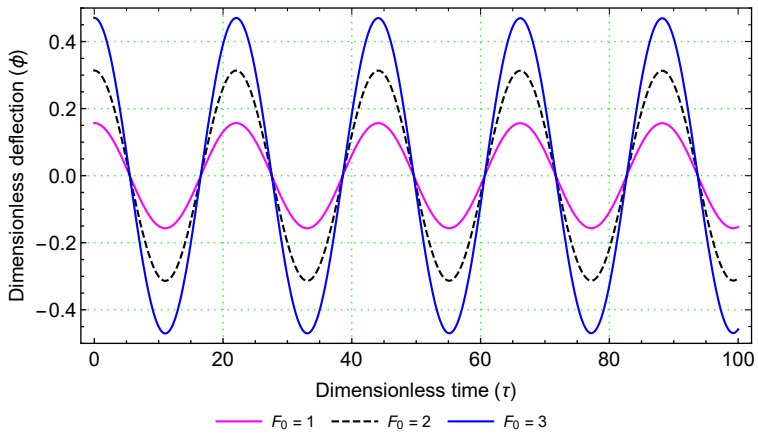


Figure 3.1.7: Variation of the dimensionless deflection with respect to dimensionless time for different values of applied load on the upper surface of the beam.

The effects of the length of the beam on the deflection under MGT theory are shown in Fig. 3.1.8. The graphs are plotted for different aspect ratios $L/h = 10$, 12, and 14.

As we see, the damping and vibration attenuates very rapidly for smaller size in length of beam resonator. Therefore, for smaller sized beam, more energy is dissipated.

Fig. 3.1.9 indicates the nature of time variation of the amplitude of thermal moment for various values of beam thickness. In the beginning, the thermal moment curve has a jump and after sometimes it attains quasi-steady vibration mode quickly. This fact also has been notified by Sun et al. (2006) for generalized thermoelasticity theory. The vibration curves of thermal moment vary by changing the thickness in different time ranges and hence, the jump of amplitude varies with the change of beam thickness. Furthermore, it can be concluded that the jump of amplitude decreases when the beam thickness decreases and the beam takes less time to reach its quasi-steady state vibration mode. The jump in amplitude increases significantly with the increase in thickness of the beam. Hence, this graph confirms the size dependency of microbeam resonator on thermoelastic damping.

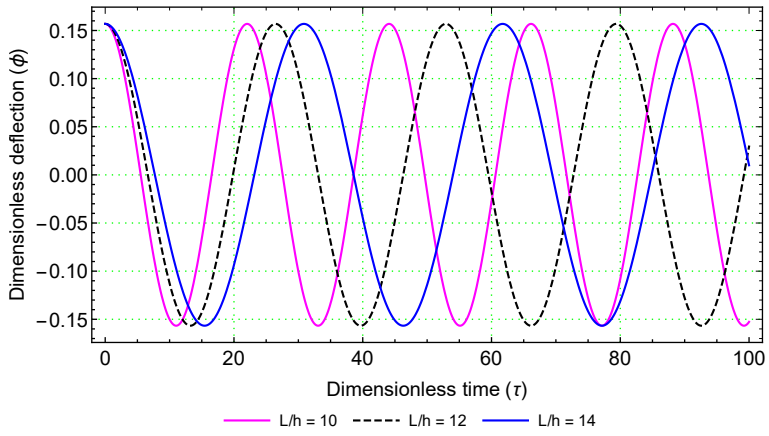


Figure 3.1.8: Variation of the dimensionless deflection with respect to dimensionless time for different values of the beam length.

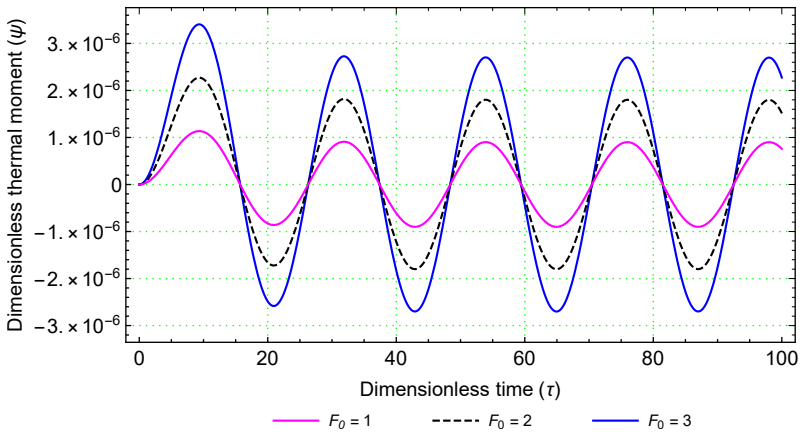


Figure 3.1.9: Variation of the dimensionless thermal moment with respect to dimensionless time for different values of the applied load on the upper surface of the beam.

Fig. 3.1.10 reveals how thermal moment is affected due to the applied load which is applied on the upper surface of the beam. To see the effects, we take the magnitude of the applied load such that $F_0 = 1$, $F_0 = 2$, and $F_0 = 3$. With the increase in the values of applied load, the amplitude of thermal moment increases and finally, reaches to a quasi-steady state vibration mode. Jump in amplitude of thermal moment increases with the increase in applied load on the beam.

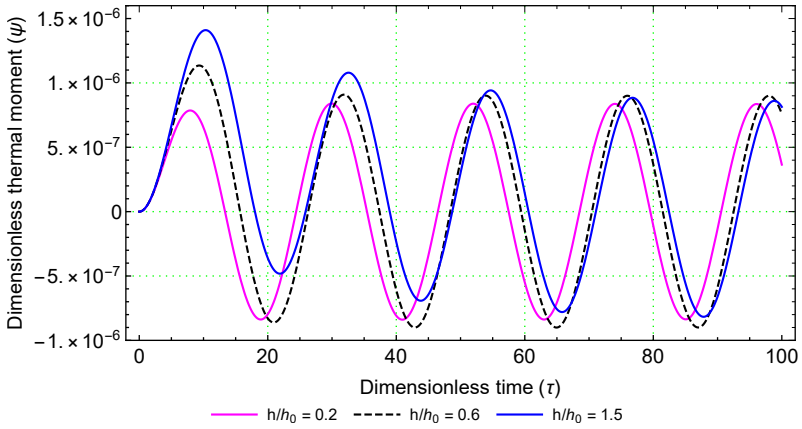


Figure 3.1.10: Variation of the dimensionless thermal moment with respect to dimensionless time for different values of the beam thickness.

The effects of beam length on vibration response of thermal moment are illustrated in Fig. 3.1.11. It is clear that the curve of thermal moment has a jump in the starting and reaches to a quasi-steady state mode with the increase of time. The amplitude of vibration frequency decreases with the increase of beam length. However, the main point here is that the frequency response of thermal moment is much faster for small beam length. In this case, the energy dissipation occurs at more faster rate.

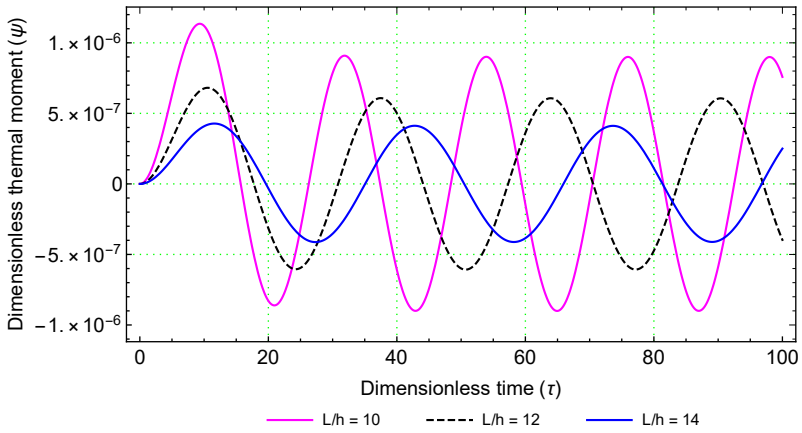


Figure 3.1.11: Variation of the dimensionless thermal moment with respect to dimensionless time for dierent values of the beam length.

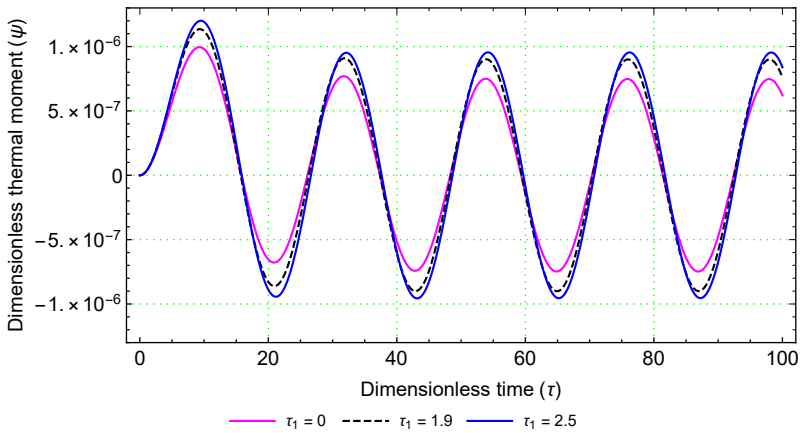


Figure 3.1.12: Effects of phase-lags on the dimensionless thermal moment with respect to the dimensionless time of the beam.

Fig. 3.1.12 displays the effects of phase-lags on the thermal moment of beam at different time. From the curve, it is observed that the vibration response of amplitude increases by increasing the values of phase-lags parameters.

### 3.1.7 Conclusion

The present section of the thesis investigates the vibration response of the deflection and thermal moment of a simply supported microbeam resonator subjected to a uniform load initially applied on the upper surface of the beam. The normalized forms of governing equations have been derived for three different coupled thermoelasticity theories (MGT, LS, and GN-III models) of microbeam in terms of the dimensionless functions, the dimensionless deflection, and the dimensionless thermal moment. The main achievements of the present work are outlined here:

- The amplitudes of deflection under all three models are approximately the same.
- There is an agreement in the results of the amplitudes of thermal moments under MGT and LS models while there is disagreement of MGT and LS models with GN-III model. The amplitudes of thermal moment of MGT and LS models are greater as compared to GN-III model.
- The amplitudes of deflection and thermal moment increases due to increasing in the magnitude of the uniform load applied on the upper surface of the beam.
- The vibration amplitudes of deflection and thermal moment attenuate at faster rate for small sized-beam, leading to more energy dissipation. This result shows that the thermoelastic damping has a size effect in the microbeam resonators. With the increase in beam thickness, the thermal moment curve shows a clear jump in amplitude and after sometimes it attains quasi-steady vibration mode quickly. Furthermore, the jump in amplitude of thermal moment increases significantly with the increase in the thickness of the beam.

- There is significant influence of phase-lag parameters on the vibration of the amplitudes of thermal moment.

## 3.2 Small-Scale Effect on Thermoelastic Vibration of Microbeam Considering Modified Couple Stress Theory and Moore-Gibson-Thompson Thermoelasticity Equation

### 3.2.1 Introduction[2]

This subchapter aims to analyze the dynamic behaviour of microbeam taking the impact of Moore-Gibson-Thompson (MGT) thermoelastic equation. In the previous subchapter, the analysis of vibration has been presented for the case when classical continuum theory is applied. However, in order to capture the small-scale effect on thermoelastic vibration of microbeams, the modified couple stress theory (MCST) is taken into account in the present work. The coupled equation of motion is derived by using the Hamilton's principle. The solutions for deflection and thermal moment of microbeams are obtained with the help of integral transform methods.

This study is an extension of the work reported by Sun et al. (2006) for the classical theory in the context of LS thermoelastic model. Recall that Sun's work have been extended by Kumar and Kumar (2019) by applying TPL heat conduction model under classical theory. In this study, we apply the MCST in order to capture the small-scale effect in microbeam resonator in the frame of MGT model. Indeed, this work is an extension of the work reported in the previous section for classical theory.

[2]The content of this subchapter is under review.

## 3.2.2 Problem formulation

### 3.2.2.1 Microbeam resonator and assumptions

Consider a small flexural deflection in an elastic thin microbeam resonator with rectangular cross-section of length $L$, width $b$, and thickness $h$ within the ambient temperature $T_0$. We assume the $x$-axis along the length direction, the $y$-axis along the width direction, and the $z$-axis along the thickness direction of the beam as displayed in Figure 3.1.1. It is also assumed that in equilibrium, the beam is unstressed and unstrained. There is no heat flow across the lower and upper surfaces of the beam so that $\partial\theta/\partial z = 0$ at $z = \pm h/2$. According to the dimension of the beam, the usual Euler-Bernoulli beam assumptions are reasonable.

### 3.2.2.2 The modified couple stress theory

The strain energy for a deformed isotropic linear elastic body occupying volume $V$ as reported by Yang et al. (2002) is given by

$$U = \int_V (\sigma_{ij}\epsilon_{ij} + m_{ij}\chi_{ij})\, dV, \quad (i, j = x, y, z) \tag{3.2.1}$$

where

$$\epsilon_{ij} = \frac{1}{2}\left(\frac{\partial u_i}{\partial x_j} + \frac{\partial u_j}{\partial x_i}\right) \tag{3.2.2}$$

$$\chi_{ij} = \frac{1}{2}\left(\frac{\partial \vartheta_i}{\partial x_j} + \frac{\partial \vartheta_j}{\partial x_i}\right) \tag{3.2.3}$$

$$\vartheta_i = \frac{1}{2}\epsilon_{ijk}u_{k,j} \tag{3.2.4}$$

in which $\epsilon_{ij}$ is the components of the strain tensor $\boldsymbol{\epsilon}$; $u_i$ is the components of the displacement vector $\boldsymbol{u}$; $\chi_{ij}$ is the components of the symmetric part of the rotation gradient tensor $\boldsymbol{\chi}$; and $\vartheta_i$ is the components of infinitesimal rotation vector $\boldsymbol{\vartheta}$. The components $m_{ij}$ of the deviatoric part of the couple stress tensor $\boldsymbol{m}$ and the components

$\sigma_{ij}$ of the stress tensor $\boldsymbol{\sigma}$ are defined by

$$m_{ij} = 2\mu l^2 \chi_{ij} \tag{3.2.5}$$

$$\sigma_{ij} = \lambda \epsilon_{kk} \delta_{ij} + 2\mu \epsilon_{ij} - (3\lambda + 2\mu)\, \alpha_T \theta \delta_{ij} \tag{3.2.6}$$

The parameter $l$ is the material length-scale parameter characterizing the couple stress effect in MCST. Due to this parameter, MCST is capable of capturing the size effect in micro structures. The constants $\mu$ and $\lambda$ are the Lame's constants given by

$$\mu = \frac{E}{2\,(1+\nu)}, \quad \lambda = \frac{E\nu}{(1+\nu)\,(1-2\nu)} \tag{3.2.7}$$

Considering plane stress condition, the nonzero components of strain and stress fields in view of Eq. (3.1.3) are expressed by

$$\epsilon_{xx} = -z \frac{\partial^2 w}{\partial x^2} \tag{3.2.8}$$

$$\sigma_{xx} = -Ez \frac{\partial^2 w}{\partial x^2} - \beta\theta \tag{3.2.9}$$

The nonzero components of rotation gradient tensor and couple stress tensor are also derived as

$$\chi_{xy} = -\frac{1}{2} \frac{\partial^2 w}{\partial x^2}, \quad m_{xy} = -\mu l^2 \frac{\partial^2 w}{\partial x^2} \tag{3.2.10}$$

#### 3.2.2.3 The MGT thermoelasticity theory

The coupled Moore-Gibson-Thompson (MGT) generalized thermoelastic equation is given by

$$\left(k \frac{\partial}{\partial t} + k^*\right) \nabla^2 \theta = \left(1 + \tau_q \frac{\partial}{\partial t}\right) \left(\rho C_v \frac{\partial^2 \theta}{\partial t^2} + T_0 \beta \frac{\partial^2 \epsilon}{\partial t^2}\right) \tag{3.2.11}$$

Eq. (3.2.11) further can be written after using Eqs. (3.2.8) and (3.2.9) as follows:

$$\left(k\frac{\partial}{\partial t}+k^{*}\right)\left(\frac{\partial^{2}\theta}{\partial x^{2}}+\frac{\partial^{2}\theta}{\partial z^{2}}\right)=\left(1+\tau_{q}\frac{\partial}{\partial t}\right)\left(\rho C_{v}\frac{\partial^{2}\theta}{\partial t^{2}}-T_{0}\beta z\frac{\partial^{4}w}{\partial t^{2}\partial x^{2}}\right) \tag{3.2.12}$$

#### 3.2.2.4 Equation of motion of microbeam based on MCST

Substituting Eqs. (3.2.8)-(3.2.10) into Eq. (3.2.1), the total strain energy considering plane stress condition takes the form

$$U=\frac{1}{2}\int_{0}^{L}\widetilde{EI}\left(\frac{\partial^{2}w}{\partial x^{2}}\right)^{2}dx+\frac{1}{2}\int_{0}^{L}\int_{-h/2}^{+h/2}b\beta\theta z\left(\frac{\partial^{2}w}{\partial x^{2}}\right)^{2}dzdx \tag{3.2.13}$$

where $\widetilde{EI}=EI+\mu Al^{2}$ is the flexural rigidity of the microbeam resonator. The kinetic energy of the beam due to its vibration is given by

$$K=\frac{1}{2}\int_{0}^{L}\rho A\left(\frac{\partial w}{\partial t}\right)^{2}dx \tag{3.2.14}$$

By introducing the Hamilton's principle, the equation of motion of the microbeam at time interval $[t_1, t_2]$ can be obtained as

$$\delta\int_{t_1}^{t_2}(U-K)\,dt=0 \tag{3.2.15}$$

Substituting Eqs. (3.2.13) and (3.2.14) into Eq. (3.2.15), the coupled equation of motion of microbeam considering MCST is expressed by

$$\widetilde{EI}\frac{\partial^{4}w}{\partial x^{4}}+\frac{\partial^{2}M_{T}}{\partial x^{2}}+\rho A\frac{\partial^{2}w}{\partial t^{2}}=0 \tag{3.2.16}$$

Eq. (3.2.12) further can be written as

$$\left(k\frac{\partial}{\partial t}+k^{*}\right)\left(\frac{\partial^{2}\theta}{\partial x^{2}}+\frac{\partial^{2}\theta}{\partial z^{2}}\right)-\left(1+\tau_{q}\frac{\partial}{\partial t}\right)\left(\rho C_{v}\frac{\partial^{2}\theta}{\partial t^{2}}-T_{0}\beta z\frac{\partial^{4}w}{\partial t^{2}\partial x^{2}}\right) \tag{3.2.17}$$

Now, integrating above equation from the range $-h/2$ to $+h/2$ with respect to $z$ after multiplying by $b\beta z$, one can obtain

$$\left(k\frac{\partial}{\partial t}+k^{*}\right)\left(\frac{\partial^{2}M_{T}}{\partial x^{2}}+b\beta\int_{-h/2}^{+h/2}\right)-\left(1+\tau_{q}\frac{\partial}{\partial t}\right)\left(\rho C_{v}\frac{\partial^{2}M_{T}}{\partial t^{2}}-T_{0}\beta^{2}I\frac{\partial^{4}w}{\partial t^{2}\partial x^{2}}\right)=0 \tag{3.2.18}$$

Using Eq. (3.1.11) into Eq. (3.2.18), the coupled governing thermoelastic equation is derived as

$$\left(k\frac{\partial}{\partial t}+k^{*}\right)\left(\frac{\partial^{2}M_{T}}{\partial x^{2}}-\frac{\pi^{2}}{h^{2}}M_{T}\right)-\left(1+\tau_{q}\frac{\partial}{\partial t}\right)\left(\rho C_{v}\frac{\partial^{2}M_{T}}{\partial t^{2}}-T_{0}\beta^{2}I\frac{\partial^{4}w}{\partial t^{2}\partial x^{2}}\right)=0 \tag{3.2.19}$$

Introducing dimensionless variables for mathematical simplicity as follows:

$$\zeta=x/L,\ \phi=w/h,\ \tau=t\varepsilon/L,\ \varepsilon=\sqrt{E/\rho},\ \psi=M_{T}h/12\widetilde{E}I,\ \tau_{1}=\tau_{q}t/L \tag{3.2.20}$$

Substituting Eq. (3.2.20) into Eqs. (3.2.16) and (3.2.19), the dimensionless form of coupled governing equations yield

$$N_{1}\frac{\partial^{4}\phi}{\partial\zeta^{4}}+N_{2}\frac{\partial^{2}\psi}{\partial\zeta^{2}}+\frac{\partial^{2}\phi}{\partial\tau^{2}}=0 \tag{3.2.21}$$

$$\left(\frac{\partial}{\partial\tau}+k_{0}\right)\left(\frac{\partial^{2}\psi}{\partial\zeta^{2}}-N_{3}\psi\right)-\left(1+\tau_{1}\frac{\partial}{\partial\tau}\right)\left(N_{4}\frac{\partial^{2}\psi}{\partial\tau^{2}}-N_{5}\frac{\partial^{4}\phi}{\partial\tau^{2}\partial\zeta^{2}}\right)=0 \tag{3.2.22}$$

The unknown coefficients of above equations are given by

$N_1 = \frac{\widetilde{EI}}{\rho A \varepsilon^2 L^2}$, $N_2 = \frac{12\widetilde{EI}}{\rho A \varepsilon^2 h^2}$, $N_3 = \pi^2 \left(\frac{L}{h}\right)^2$, $N_4 = \frac{\rho C_v \varepsilon h L}{k}$, $N_5 = \frac{EIT_0\beta^2 h^2}{12k\rho\varepsilon L\widetilde{EI}}$.

In order to solve the coupled governing equations (3.2.21) and (3.2.22) for deflection and thermal moment of the microbeam, we consider the initial as well as boundary conditions as follows. It is assumed that initially a load of magnitude $F_0$ is applied uniformly to the upper surface of the beam. Thus, the initial conditions at time $\tau = 0$ can be assumed as

$$\begin{gathered} \phi = F_0\left(\zeta - 2\zeta^2 + \zeta^4\right),\ \frac{\partial\phi}{\partial\tau} = \frac{\partial^2\phi}{\partial\tau^2} = 0 \\ \psi = \frac{\partial\psi}{\partial\tau} = \frac{\partial^2\psi}{\partial\tau^2} = 0 \end{gathered} \tag{3.2.23}$$

We also consider that both the ends of the beam are simply supported. Then, the boundary conditions at $\zeta = 0$ and $\zeta = 1$ are given by

$$\phi = \frac{\partial^2\phi}{\partial\zeta^2} = 0,\ \psi = 0 \tag{3.2.24}$$

### 3.2.3 Solution for deflection and thermal moment of microbeam

The governing equations (3.2.21) and (3.2.22) are difficult to solve when the thermoelastic coupling effect is taken into account. Therefore, the integral transformation method in this paper is used to obtain the solution for deflection and thermal moment of the microbeam. Thus, the finite sine Fourier transform of $\phi$ and $\psi$ at $\zeta = 0$ and $\zeta = 1$ can be given by

$$\begin{gathered} \phi_m(m,\tau) = \int_0^1 \phi(m,\tau)\, sin\left(r_m\zeta\right) d\zeta \\ \psi_m(m,\tau) = \int_0^1 \psi(m,\tau)\, sin\left(r_m\zeta\right) d\zeta \end{gathered} \tag{3.2.25}$$

Based on the Fourier series theory, the inversion of Eq. (3.2.25) can be expressed by

$$\begin{aligned}\phi(\zeta,\tau) &= 2\sum_{m=1,3,..}^{\infty}\phi_m(m,\tau)\,sin(r_m\zeta)\,d\zeta \\ \psi(\zeta,\tau) &= 2\sum_{m=1,3,..}^{\infty}\psi_m(m,\tau)\,sin(r_m\zeta)\,d\zeta\end{aligned} \tag{3.2.26}$$

Now, applying the transformation of Eq. (3.2.25) into Eqs. (3.2.21) and (3.2.22) gives

$$N_1 r_m^4\phi_m - N_2 r_m^2\psi_m + \frac{\partial^2\phi_m}{\partial\tau^2} = 0 \tag{3.2.27}$$

$$\left(\frac{\partial}{\partial\tau}+k_0\right)\left(r_m^2\psi_m + N_3\psi_m\right) + \left(1+\tau_1\frac{\partial}{\partial\tau}\right)\left(N_4\frac{\partial^2\psi_m}{\partial\tau^2} + r_m^2 N_5\frac{\partial^2\phi_m}{\partial\tau^2}\right) = 0 \tag{3.2.28}$$

And the initial conditions at $\tau = 0$ takes the form

$$\begin{aligned}\phi_m = \tfrac{48}{r_m^5}F_0,\ \tfrac{\partial\phi_m}{\partial\tau} = \tfrac{\partial^2\phi_m}{\partial\tau^2} = 0 \\ \psi_m = \tfrac{\partial\psi_m}{\partial\tau} = \tfrac{\partial^2\psi_m}{\partial\tau^2} = 0\end{aligned} \tag{3.2.29}$$

In order to solve Eqs. (3.2.27) and (3.2.28) with the help of initial conditions (3.2.29), the Laplace transform technique is used. Thus, the deflection $\phi_m$ from Eqs. (3.2.27) and (3.2.28) in the Laplace transform domain is obtained as

$$\overline{\phi}_m(m,s) = \frac{48F_0}{r_m^5}\left(\frac{k_1 s + k_2 s^2 + k_3 s^3 + k_4 s^4}{\overline{k}_0 + \overline{k}_1 s + \overline{k}_2 s^2 + \overline{k}_3 s^3 + \overline{k}_4 s^4 + \overline{k}_5 s^5}\right) \tag{3.2.30}$$

The unknown coefficients of above equation are given by

$k_1 = k_0'\left(r_m^2 + N_3\right) - N_2 N_5 r_m^4,\ k_2 = \left(r_m^2 + N_3\right) - \tau_0 N_2 N_5 r_m^4,\ k_3 = N_4,\ k_4 = \tau_0 N_4,$
$\overline{k}_0 = k_0'\left(r_m^2 + N_3\right) N_1 r_m^4,\ \overline{k}_1 = \left(r_m^2 + N_3\right) N_1 r_m^4,\ \overline{k}_2 = k_0'\left(r_m^2 + N_3\right) + \left(N_1 N_4 - N_2 N_5\right) r_m^4,$
$\overline{k}_3 = \left(r_m^2 + N_3\right) + \left(N_1 N_4 + N_2 N_5\right)\tau_1 r_m^4,\ \overline{k}_4 = N_4,\ \overline{k}_5 = \tau_1 N_4.$

Taking inversion of the Laplace transform of Eq. (3.2.30), the solution for $\phi_m$ in time domain is derived as

$$\phi_m(m,\tau) = \frac{48F_0}{r_m^5}\sum_{\alpha}\left(\frac{k_1\alpha + k_2\alpha^2 + k_3\alpha^3 + k_4\alpha^4}{\overline{k}_1 + 2\overline{k}_2\alpha + 3\overline{k}_3\alpha^2 + 4\overline{k}_4\alpha^3 + 5\overline{k}_5\alpha^4}\right)e^{\alpha\tau} \tag{3.2.31}$$

where $\alpha$ represents the all solutions of the equation $\overline{k}_0+\overline{k}_1\alpha+\overline{k}_2\alpha^2+\overline{k}_3\alpha^3+\overline{k}_4\alpha^4+\overline{k}_5\alpha^5 = 0$. Using Eq. (3.2.26), the required solution for dimensionless deflection is obtained as

$$\phi(\zeta,\tau) = 96\sum_{m=1,3,..}\frac{1}{r_m^5}\sum_{\alpha}\left(\frac{k_1\alpha+k_2\alpha^2+k_3\alpha^3+k_4\alpha^4}{\overline{k}_1+2\overline{k}_2\alpha+3\overline{k}_3\alpha^2+4\overline{k}_4\alpha^3+5\overline{k}_5\alpha^4}\right)e^{\alpha\tau}sin(r_m\zeta) \tag{3.2.32}$$

Similarly, the solution for dimensionless thermal moment ($\psi$) can be derived.

### 3.2.4 Numerical results and discussion

This section is devoted to analyze the thermoelastic vibration of microbeam resonator, made of silicon material on the basis of the analytical results as obtained above in the frame of MCST and recently developed MGT thermoelastic model. The size-dependent solutions for deflection and thermal moment of microbeam have been derived by considering the case when a uniform load is applied to the upper surface of the beam. The variations of deflection and thermal moment as a function of time has been investigated in detail. The results obtained under MCST are compared to the results of classical theory as special case when material length-scale parameter ($l$) is zero. Further, the present results are compared to the corresponding results of LS and GN-III models under the impact of MCST. The properties of silicon resonator at reference temperature $293K$ are given below (Sun et al., 2006):

$\rho = 2330\,Kg/m^3$, $E = 169\,GPa$, $\nu = 0.22$, $k = 156\,Wm^{-1}K^{-1}$, $\alpha_T = 2.59\times 10^{-6}K^{-1}$, $C_v = 713\,JKg^{-1}K^{-1}$, $k^* = 156\,Wm^{-1}K^{-1}s^{-1}$.

In order to analyze the thermoelastic vibration, the dimension of microbeam, in this work, is set to $L/h = 10$, $b/h = 0.5$ in which $h = 10\mu m$. Also, the relaxation time $\tau_q$ associated with MGT thermoelastic heat equation is set to in its dimensionless form $\tau_1$ as 1.9. The aspect ratio of material length-scale parameter to thickness of the beam is fixed to $l/h = 0.2$ excluding in Figure 3.2.3. The numerical results are shown in dimensionless time range $\tau = 0-100$. The obtained results are analyzed in the

following subsections:

#### 3.2.4.1 Results validation

The variations of dimensionless deflection ($\phi$) and thermal moment ($\psi$) as a function of dimensionless time ($\tau$) are displayed in Figs. 3.2.1 and 3.2.2. This subsection shows a comparison between the results under classical theory and MCST as well as among the predictions by different thermoelastic models namely, MGT, GN-III, and LS models. For the validation of the present results, the work reported by Sun et al. (2006) for classical theory in the frame of LS model is taken into consideration.

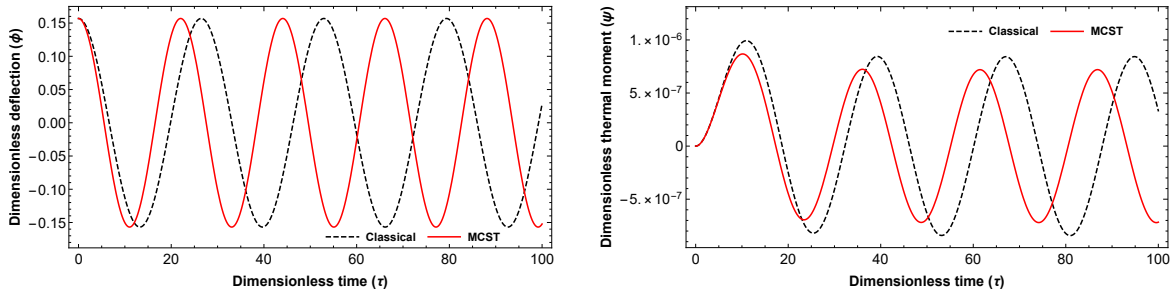


Figure 3.2.1: Variation of deflection and thermal moment versus time under classical theory and MCST.

Figure 3.2.1 ($a$) indicates that there is a significant effect of material length-scale parameter on deflection. The amplitude of deflection under classical theory becomes faster than MCST as time increases, while the peak value remains approximately the same under both the theories. This shows that the phase difference of the vibration between these two theories increase with time. Figure 3.2.1 ($b$) illustrates the variation of thermal moment against time under classical and MCST theories. It is observed that there is a jump of the amplitude in the starting under both the theories, thereafter the vibration reaches to a steady state mode. The phase difference of moment between the curves of classical theory and MCST is also increases with time. It is further noticed that the amplitude of thermal moment is greater under MCST in comparison to the classical theory. For small time range, the vibration of thermal moment under both the

theories is approximately the same, while it becomes more significant as time increases. The response of moment due to modeling under classical theory indicates slow energy decay than the modeling under MCST.

The time variation of deflection is shown in Figure 3.2.2 $(a)$ considering MGT, GN-III, and LS thermoelastic models. It can be seen from the Figure that vibration response of deflection under these three models are approximately the same. Moreover, it can be concluded that phase-lag effect is negligible on the vibration response of deflection with respect to time. Figure 3.2.2 $(b)$ shows the vibration response of thermal moment under MGT, GN-III, and LS models as a function of time. It is seen that thermal moment curves of MGT and LS models almost match together, while there is prominent difference in the plots of these two models and of the GN-III model. However, in the starting under all models, the jump can be observed. The amplitude of thermal moment curve of GN-III model is lower than the amplitude MGT and LS models. It is illustrated that the frequency response of thermal moment becomes more faster under GN-III model as compared to MGT and LS models as time increases. This shows that the vibration of thermal moment under GN-III model is smaller than MGT and LS models due to more energy dissipation.

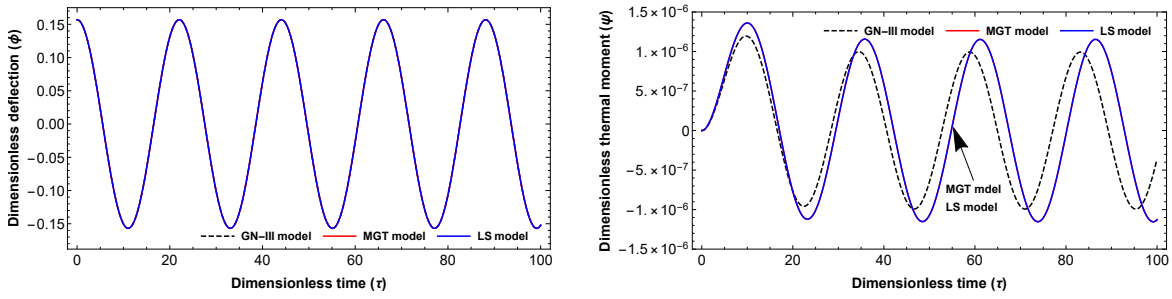


Figure 3.2.2: Variation of deflection and thermal moment under MGT, GN-III, and LS models.

#### 3.2.4.2 Effect of length-scale parameter

This section is presented to analyze the impact of material length-scale parameter on deflection and thermal moment under MGT thermoelastic model. The results are shown for various values of $l$ ($l/h = 0,\ 0.2,\ 0.4$). Figure 3.2.3 $(a)$ demonstrates that the attenuation of deflection changes with the change of the material length-scale parameter. However, the peak value of the thermal moment curve remains approximately the same. From the Figure, it may be concluded that when the material length-scale parameter approaches to the critical thickness of the beam, the attenuation becomes stronger. It means when the value of material parameter increases, the vibration offers greater rate of energy dissipation. Hence, the vibration of the microbeam will remain for a smaller time in this case. Figure 3.2.3 $(b)$ indicates that the thermal moment curve has jump in the beginning and then reaches quasi-steady state mode of vibration quickly. It is seen that when the material length-scale parameter increases, the amplitude of thermal moment curve increases. The jump varies with the change of material length-scale parameter. When the value of material parameter decreases, the attenuation becomes faster leading to low energy dissipation in the vibrating microbeam resonator. Further, the phase difference also changes with time by increasing the material length-scale parameter. Hence, the material length-scale parameter can be selected as small when developing the microbeam resonator so that the vibration can last longer.

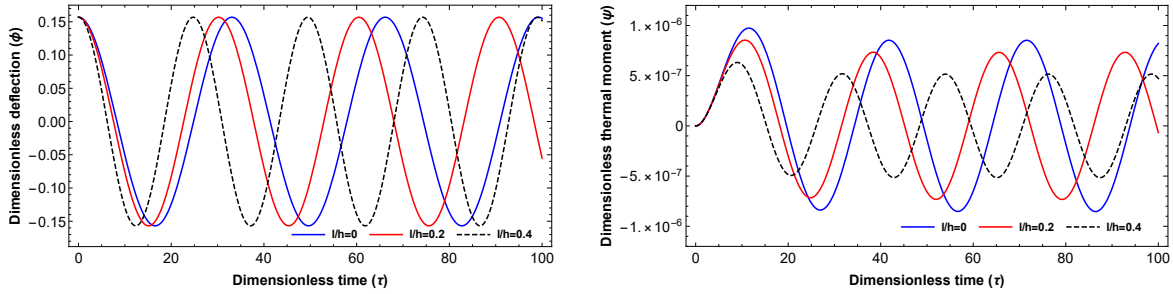


Figure 3.2.3: Variation of deflection and thermal moment versus time for different values of length-scale parameter.

### 3.2.5 Conclusion

In the present subchapter, we analyze the thermoelastic vibration response of microbeam resonator considering MCST in the frame of MGT heat conduction model. The expressions of dimensionless deflection and thermal moment are obtained for a simply supported microbeam on which a uniform load is applied to the upper surface. The main conclusions as observed under this investigation can be reported as follows:

- When MCST is used instead of classical theory, the attenuation of deflection and thermal moment is stronger.
- The vibration response of the microbeam lasts longer for small value of the material length-scale parameter.
- The phase-lag time has no influence on deflection but has a substantial effect on the thermal moment curve.
- The response of the thermal moment in the MGT and LS models is nearly same, but differs from the GN-III model.
- The vibration curve for the GN-III model has a faster decrease of energy than the MGT and LS models.

## 3.3 Surface Energy Effects on Thermoelastic Vibration of Nanomechanical Systems under Moore-Gibson-Thompson Thermoelasticity and Eringen's Nonlocal Elasticity Theories

### 3.3.1 Introduction[3]

Surface and size effects are frequently important in the design of high-performance nano-sized devices. However, due to the lack of the small-scale impact, the classical theory fails to predict the size-dependent behavior of nano devices. In this regard, the current subchapter attempts to investigate the dynamic and mechanical behaviours of nanobeams using nonlocal elasticity theory and the recently proposed Moore-Gibson-Thompson (MGT) thermoelasticity theories while taking into account of surface energy effects in the problem formulation. Experimental studies have shown that small-scale structures behave differently than their macro counterparts (Chen et al., 2006; Hepplestone et al., 2006). These variations can be attributed to surface effects, quantum effects, and/or increase in defect density from the classical result, all of which become noticeable at small-scales. In case of micro/nano-sized structures that involve higher range of surface to-bulk ratio and the number of atoms is big enough, the atoms of the free surface of a body experience a more dissimilar circumference than the atoms of the bulk. The influence of surface and the surface forces therefore become significant. The surplus energy associated with the atoms of the surface of the body is named as the surface free energy. To investigate the influence of surface effects on the elastic behavior of small-scale structures, some models have therefore been developed that consider the terms like surface density, surface stress and surface elasticity. Gurtin and Murdoch's

[3]The content of this subchapter is published in ***European Journal of Mechanics-A/Solids***, (2022):104530.

(1975; 1978) models have been widely utilized to investigate the influence of surface elasticity on the mechanical behavior of small scale structures (Sharma et al., 2003; Tian and Rajapakse, 2007; Wang and Feng, 2009; Chiu and Chen, 2011). Hamidi et al. (2020) investigated TED in silver nanobeam resonators using Green-Naghdi thermoelasticity and nonlocal elasticity theories by taking into account the surface energy effects. Using surface elasticity theory, Ru (2009) investigated the size effects on TED of vibrating beams. Dixit et al. (2013) discussed about the surface effects on TED in nanobeam resonators and obtained a simplified expression of the quality factor. Ma et al. (2010) investigated the effects of surface on the pull-in instability of electrostatic switches in an Euler–Bernoulli beam, including surface elasticity and residual surface stress. Shi et al. (2017) developed a coupled linear two-dimensional magneto-electro-thermoelastic laminated plate theory that takes nonlocal and surface effects into account, based on the virtual work principle and Mindlin's theory. The size effects of specific heat and elastic modulus on TED of geometrically nonlinear beams have been discussed recently by Dixit and Gaonkar (2021).

On the basis of the works reported in the literature, this subchapter focuses on the development of a analytical model to study the vibrational response of nanomechanical resonators considering surface energy effects. In the context of nonlocal elasticity and surface elasticity theories, the governing equation of motion for an Euler-Bernoulli nanobeam that is simply supported at both ends and has a uniform load on the top surface is first derived. Thereafter, the solution for deflection and temperature distribution along the thickness direction of the nanobeam is obtained based on MGT theory using the finite Fourier sine transform and Laplace transform techniques. The influences of nonlocal parameter, phase-lag time, residual surface tension, surface elastic modulus, thickness and length of the nanobeam on deflection and temperature over time are systematically analyzed in depth. Some important points are highlighted regarding size dependency and surface effects on vibration of nanobeams in the present context.

When surface and small-scale effects are included, this approach may be valuable in understanding the dynamic and mechanical behaviors of nanomechanical systems.

### 3.3.2 Problem formulation

#### 3.3.2.1 Beam deformation considering surface effects

The surface effects on the dynamic and mechanical behavior of nanodevices are calculated by taking into account the surface stresses or surface energy. As described by Cammarata (1994) and Gibbs (1906), the planar stress tensor $\sigma_{ij}$ depends on the density $\gamma$ of surface energy and surface strain tensor $\epsilon_{ij}^{s}$ as

$$\sigma_{ij} = \gamma\delta_{ij} + \frac{\partial\gamma}{\partial\epsilon_{ij}^{s}} \tag{3.3.1}$$

The linear form of above equation is written as

$$\sigma^{s} = \sigma^{0} + E^{s}\epsilon \tag{3.3.2}$$

where $\sigma^{0}$ is the residual surface tension in the absence of strain, and $E^{s}$ denotes the surface elasticity modulus (Jing et al., 2006; Miller and Shenoy, 2000).

For calculating deflection of an Euler–Bernoulli beam, the bending moment $EI$ plays a significant role, where $E$ and $I$ stand for Young's modulus and moment of inertia, respectively. By considering surface effects taken into account, the bending strength $EI$ is derived as (see Wang and Feng, 2009)

$$(EI)^{*} = EI + \frac{1}{2}E^{s}bh^{2} + \frac{1}{6}E^{s}h^{3} \tag{3.3.3}$$

According to Young–Laplace (Gurtin et al., 1998; Chen et al., 2006), the stress jump $\left\langle \sigma_{ij}^{+} - \sigma_{ij}^{-} \right\rangle$ in a part of the surface is related to the curvature tensor $\kappa$ of the surface by

$$\left\langle \sigma_{ij}^{+} - \sigma_{ij}^{-} \right\rangle n_i n_j = \sigma^0 \kappa \tag{3.3.4}$$

where $\sigma_{ij}^{+}$ and $\sigma_{ij}^{-}$ denote the stresses above and below the surface, respectively, and $n_i$ is the surface normal unit vector. The second derivative of deflection $w(x)$ at position $x$ is approximated as $w''(x)$, which indicates the curvature in bending of the beam. It is worth noting that the second derivative of deflection becomes $w''(x) = 0$ in an unchanged configuration. In this case, the structure will not be affected by the residual surface stress. A deflected beam creates residual surface tension in the form of longitudinally distributed transverse load. The transverse load $f(x)$ predicted by Young–Laplace equation is given by (Wang and Feng, 2007; 2009)

$$f(x) = H \frac{\partial^2 w(x)}{\partial x^2} \tag{3.3.5}$$

where $H$ is a constant depends on the area of cross-section and residual surface tension of the beam. For a thin beam with rectangular cross-sectional shape, $H$ is derived as (Wang and Feng, 2007; He and Lilley, 2008)

$$H = 2\sigma^0 b \tag{3.3.6}$$

#### 3.3.2.2 The Euler-Bernoulli beam theory

In this section, a nano-sized Euler-Bernoulli beam with rectangular cross-section $A = b \times h$ of dimension; width $b\,(-b/2 \leq y \leq +b/2)$, thickness $h\,(-h/2 \leq z \leq +h/2)$, and length $L\,(0 \leq x \leq L)$ is considered as displayed in Figure 3.3.1. The nanobeam is simply supported at both ends, and a uniform load $F$ is assumed to be acting on the upper surface of the nanobeam. Initially, at the reference temperature $T_0 = 293\,K$, the beam is assumed to be unstressed and unstrained. The equilibrium equations for an

Euler-Bernoulli beam is derived as (Rao, 2007)

$$\frac{\partial^2 M}{\partial x^2} + f = \rho A \frac{\partial^2 w}{\partial t^2} \tag{3.3.7}$$

in which $M$ denotes the bending moment that can be derived on the consideration of surface effects as follows (Wang and Feng, 2009):

$$M = -(EI)^* \frac{\partial^2 w}{\partial x^2} \tag{3.3.8}$$

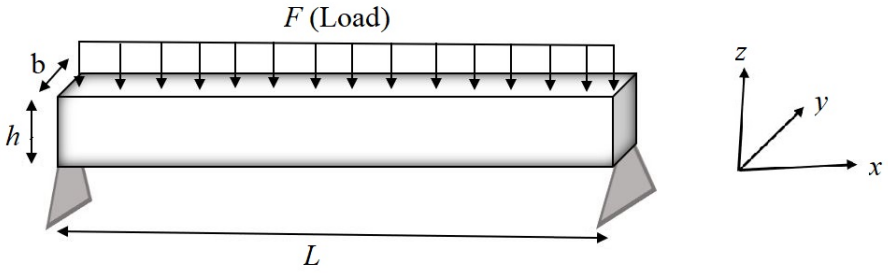


Figure 3.3.1: Simply supported nonlocal Euler-Bernoulli nanobeam with uniform load on the upper surface.

#### 3.3.2.3 Nonlocal elasticity theory in an Euler-Bernoulli beam

The constitutive relationship between classical and nonlocal stresses in differential form is described according to Eringen's nonlocal elasticity theory as follows (Eringen, 1983; Eringen and Edelen, 1972):

$$\sigma_{xx}^{nl} - (e_0 a)^2 \frac{\partial^2 \sigma_{xx}^{nl}}{\partial x^2} = \sigma_{xx}^{l} \tag{3.3.9}$$

where $\sigma_{xx}^{l}$ represents the classical (local) stress and $\sigma_{xx}^{nl}$ is the nonlocal stress. The quantity $e_0 a$ stands for the nonlocal parameter that determines the size effect, in which

$e_0$ and $a$ respectively denote the material constant and external characteristic length. The stress strain relation for the Euler–Bernoulli beam model including the temperature effect is as follows (Hetnarski et al., 2009):

$$\sigma_{xx}^{l} = E\epsilon_{xx} - \beta\theta \tag{3.3.10}$$

On substitution of Eq. (3.3.10) into Eq. (3.3.9), the stress-strain equation can be obtained as

$$\sigma_{xx}^{nl} - (e_0 a)^2 \frac{\partial^2 \sigma_{xx}^{nl}}{\partial x^2} = E\epsilon_{xx} - \beta\theta \tag{3.3.11}$$

The relationship for the bending moment utilizing surface effects and nonlocal elasticity theory is as follows:

$$M^{nl} - (e_0 a)^2 \frac{\partial^2 M^{nl}}{\partial x^2} = -(EI)^* \frac{\partial^2 w}{\partial x^2} - M_T \tag{3.3.12}$$

The Eq. (3.3.12) further can be written as

$$\frac{\partial^2 M_{nl}}{\partial x^2} - (e_0 a)^2 \frac{\partial^4 M^{nl}}{\partial x^4} = -(EI)^* \frac{\partial^4 w}{\partial x^4} - \frac{\partial^2 M_T}{\partial x^2} \tag{3.3.13}$$

Using Eq. (3.3.7) into Eq. (3.3.13) yields

$$\rho A \frac{\partial^2 w}{\partial t^2} - H \frac{\partial^2 w}{\partial x^2} + (EI)^* \frac{\partial^4 w}{\partial x^4} = (e_0 a)^2 \left( \rho A \frac{\partial^4 w}{\partial t^2 \partial x^2} - H \frac{\partial^4 w}{\partial x^4} \right) - \frac{\partial^2 M_T}{\partial x^2} \tag{3.3.14}$$

Clearly the above equation is the more extended form of the equation of motion for an Euler-Bernoulli nanobeam that takes nonlocal elasticity and surface effects into account. In particular, the above equation will be simplified to the equation of motion for classical Euler-Bernoulli beam model if $\sigma^0 = 0$, $E^s = 0$, and $e_0 a = 0$.

#### 3.3.2.4 Equations of coupled thermoelasticity based on MGT theory

Like previous subchapters, we consider here the coupled governing heat conduction equation based on the Moore-Gibson-Thompson (MGT) theory of thermoelasticity that is given by

$$\left(k\frac{\partial}{\partial t}+k^{*}\right)\nabla^{2}\theta=\left(1+\tau_{q}\frac{\partial}{\partial t}\right)\left(\rho C_{v}\frac{\partial^{2}\theta}{\partial t^{2}}+T_{0}\beta\frac{\partial^{2}\epsilon}{\partial t^{2}}\right) \tag{3.3.15}$$

The equation (3.3.15) further can be expressed as

$$\left(k\frac{\partial}{\partial t}+k^{*}\right)\left(\frac{\partial^{2}\theta}{\partial x^{2}}+\frac{\partial^{2}\theta}{\partial z^{2}}\right)=\left(1+\tau_{q}\frac{\partial}{\partial t}\right)\left(\rho C_{v}\frac{\partial^{2}\theta}{\partial t^{2}}-T_{0}\beta z\frac{\partial^{4}w}{\partial t^{2}\partial x^{2}}\right) \tag{3.3.16}$$

Multiplying above equation with $b\beta z$ at both sides, then integrating over the thickness of the beam with respect to $z$, we get

$$\left(k\frac{\partial}{\partial t}+k^{*}\right)\left(\frac{\partial^{2}M_{T}}{\partial x^{2}}+b\beta\int_{-h/2}^{+h/2}z\frac{\partial^{2}\theta}{\partial z^{2}}dz\right)=\left(1+\tau_{q}\frac{\partial}{\partial t}\right)\left(\rho C_{v}\frac{\partial^{2}M_{T}}{\partial t^{2}}-IT_{0}\beta^{2}\frac{\partial^{4}w}{\partial t^{2}\partial x^{2}}\right) \tag{3.3.17}$$

Along the thickness direction of the nanobeam, it is assumed that the temperature increment $\theta$ varies in terms of $sin\,(Pz)$ function due to very thin beam structure in which $P=\pi/h$ (Sun et al., 2006). Therefore, the temperature increment can be expressed as

$$\theta\,(x,z,t)=\theta_{0}\,(x,t)\,sin\,(Pz) \tag{3.3.18}$$

Inserting Eq. (3.3.18) into Eq. (3.3.17), we get

$$\rho A\frac{\partial^2 w}{\partial t^2} - H\frac{\partial^2 w}{\partial x^2} + (EI)^* \frac{\partial^4 w}{\partial x^4} - (e_0 a)^2 \left(\rho A\frac{\partial^4 w}{\partial t^2 \partial x^2} - H\frac{\partial^4 w}{\partial x^4}\right) - \frac{2b\beta}{P^2}\frac{\partial^2 \theta_0}{\partial x^2} = 0 \quad (3.3.19)$$

$$\left(k\frac{\partial}{\partial t} + k^*\right)\left(\frac{\partial^2 \theta_0}{\partial x^2} - P^2\theta_0\right) - \left(1 + \tau_q\frac{\partial}{\partial t}\right)\left(\rho C_v\frac{\partial^2 \theta_0}{\partial t^2} - \frac{IT_0\beta p^2}{2b}\frac{\partial^4 w}{\partial t^2 \partial x^2}\right) = 0 \quad (3.3.20)$$

For mathematical simplification, the dimensionless variables are defined as

$$\zeta = \frac{x}{L},\ \phi = \frac{w}{h},\ \tau = \frac{t\varepsilon}{L},\ \varepsilon = \sqrt{\frac{E}{\rho}},\ \theta_1 = \frac{\theta_0}{T_0},\ \tau_1 = \frac{\tau_q \varepsilon}{L},\ \Omega = \frac{e_0 a}{L} \quad (3.3.21)$$

in which $\phi$ and $\theta_1$ are used for dimensionless deflection and dimensionless temperature of the beam, respectively. Inserting Eq. (3.3.21) into Eqs. (3.3.19) and (3.3.20), the non-dimensional form of coupled governing equations are derived as

$$\frac{\partial^2 \phi}{\partial \tau^2} - S_1\frac{\partial^2 \phi}{\partial \zeta^2} + S_2\frac{\partial^4 \phi}{\partial \zeta^4} - S_3\frac{\partial^4 \phi}{\partial \tau^2 \partial \zeta^2} - S_4\frac{\partial^2 \theta_1}{\partial \zeta^2} = 0 \quad (3.3.22)$$

$$\left(k_0 + \frac{\partial}{\partial \tau}\right)\left(\frac{\partial^2 \theta_1}{\partial \zeta^2} - M_2\theta_1\right) - \left(1 + \tau_1\frac{\partial}{\partial \tau}\right)\left(S_5\frac{\partial^2 \theta_1}{\partial \tau^2} - S_6\frac{\partial^4 \phi}{\partial \tau^2 \partial \zeta^2}\right) = 0 \quad (3.3.23)$$

where $S_1 = \frac{H}{EA}$, $S_2 = \frac{1}{EA}\left(\Omega^2 H + \frac{(EI)^*}{L^2}\right)$, $S_3 = \Omega^2$, $S_4 = \frac{2T_0 b\beta}{P^2 EAh}$, $S_5 = \frac{\rho C_v EL\varepsilon}{k}$, $S_6 = \frac{\beta I P^2 h\varepsilon}{2bkL}$.

### 3.3.3 Solution for deflection and temperature

In order to solve the governing equations (3.3.22) and (3.3.23) with the thermoelastic coupling effect we adopt the same procedure as followed by Sun et al. (2006). Therefore, Laplace transform together with finite Fourier sine transform method is employed

to obtain the expressions for deflection and temperature of nanobeam. For simply supported nanobeam with isothermal ends, the initial conditions at $\tau = 0$ are considered as (Sun et al., 2006)

$$\phi = F_0\left(\zeta - 2\zeta^2 + \zeta^4\right),\ \frac{\partial\phi}{\partial\tau} = \frac{\partial^2\phi}{\partial\tau^2} = \frac{\partial^3\phi}{\partial\tau^3} = 0,\ \theta_1 = \frac{\partial\theta_1}{\partial\tau} = \frac{\partial^2\theta_1}{\partial\tau^2} = \frac{\partial^3\theta_1}{\partial\tau^3} = 0 \quad (3.3.24)$$

where $F_0$ is the magnitude of uniform applied load $F$ on the beam. The corresponding boundary conditions at both ends $\zeta = 0$ and $\zeta = 1$ are assumed to be

$$\phi = \frac{\partial^2\phi}{\partial\zeta^2} = 0,\ \theta_1 = 0 \quad (3.3.25)$$

Now, taking the finite Fourier sine transform on both sides to Eqs. (3.3.22) and (3.3.23), one can obtain in view of Eq. (3.3.25)

$$\left(r_m^2 S_1 + r_m^4 S_2\right)\phi_m + \left(1 + r_m^2 S_3\right)\frac{\partial^2\phi_m}{\partial\tau^2} + r_m^2 S_4\theta_{1m} = 0 \quad (3.3.26)$$

$$\left(k_0 + \frac{\partial}{\partial\tau}\right)\left(r_m^2\theta_{1m} + M_2\theta_{1m}\right) - \left(1 + \tau_1\frac{\partial}{\partial\tau}\right)\left(S_5\frac{\partial^2\theta_{1m}}{\partial\tau^2} + S_6 r_m^2\frac{\partial^2\phi_m}{\partial\tau^2}\right) = 0 \quad (3.3.27)$$

The term $\theta_{1m}$ denotes the Fourier transform of $\theta_1$. And corresponding the initial conditions (3.3.24) take the form

$$\phi = \frac{48}{r_m^5}F_0,\ \frac{\partial\phi_m}{\partial\tau} = \frac{\partial^2\phi_m}{\partial\tau^2} = \frac{\partial^3\phi_m}{\partial\tau^3} = 0,\ \theta_{1m} = \frac{\partial\theta_{1m}}{\partial\tau} = \frac{\partial^2\theta_{1m}}{\partial\tau^2} = \frac{\partial^3\theta_{1m}}{\partial\tau^3} = 0 \quad (3.3.28)$$

Applying the Laplace transform to both sides of Eqs. (3.3.26) and (3.3.27), then using Eq. (3.3.28) lead to

$$\left\{r_m^2 S_1 + r_m^4 S_2 + \left(1 + r_m^2 S_3\right) s^2\right\} \overline{\phi}_m + \left\{r_m^2 S_4\right\} \overline{\theta}_{1m} = \frac{48}{r_m^5} F_0 \left(1 + r_m^2 S_3\right) s \qquad (3.3.29)$$

$$\left\{k_0 \left(r_m^2 + M_2\right) + \left(r_m^2 + M_2\right) s + S_5 s^2 + S_5 \tau_1 s^3\right\} \overline{\theta}_{1m} + \left\{r_m^2 S_6 s^2 + r_m^2 \tau_1 s^3\right\} \overline{\phi}_m = \frac{48}{r_m^5} F_0 S_6 r_m^2 \left(1 + \tau_1 s\right) s \qquad (3.3.30)$$

where, $\overline{\theta}_{1m}$ represents the Laplace transform of $\theta_{1m}$. From Eqs. (3.3.29) and (3.3.30), one can derive the expression for deflection of the nanobeam as follows:

$$\overline{\phi}_m (m, s) = \frac{48}{r_m^5} F_0 \left( \frac{v_0 + v_1 s + v_2 s^2 + v_3 s^3 + v_4 s^4}{\overline{v}_0 + \overline{v}_1 s + \overline{v}_2 s^2 + \overline{v}_3 s^3 + \overline{v}_4 s^4 + \overline{v}_5 s^5} \right) \qquad (3.3.31)$$

where $\alpha_0 = 1 + S_3 r_m^2$, $\beta_0 = M_2 + r_m^2$, $v_0 = 0$, $v_1 = k_0' \alpha_0 \beta_0 - S_4 S_6 r_m^2$, $v_2 = \alpha_0 \beta_0 - \tau_1 S_4 S_6 r_m^4$, $v_3 = \alpha_0 S_5$, $v_4 = \tau_1 \alpha_0 S_5$, $\overline{v}_0 = k_0' \beta_0 \left(S_1 + S_2 r_m^2\right) r_m^2$, $\overline{v}_1 = \beta_0 \left(S_1 + S_2 r_m^2\right) r_m^2$, $\overline{v}_2 = k_0' \alpha_0 \beta_0 + S_5 \left(S_1 + S_2 r_m^2\right) r_m^2 - S_4 S_6 r_m^4$, $\overline{v} = \alpha_0 \beta_0 + \tau_1 S_5 \left(S_1 + S_2 r_m^2\right) r_m^2 - \tau_1 S_4 S_6 r_m^4$, $\overline{v}_4 = \alpha_0 S_5$, $\overline{v}_5 = \tau_1 \alpha_0 S_5$.

Taking inverse Laplace transform of Eq. (3.3.31), one can obtain the solution for deflection $\phi_m$ as follows:

$$\phi_m (m, \tau) = \frac{48}{r_m^5} F_0 \sum_{\alpha} \left( \frac{v_0 + v_1 \alpha + v_2 \alpha^2 + v_3 \alpha^3 + v_4 \alpha^4}{\overline{v}_1 + 2\overline{v}_2 \alpha + 3\overline{v}_3 \alpha^2 + 4\overline{v}_4 \alpha^3 + 5\overline{v}_5 \alpha^4} \right) e^{\alpha \tau} \qquad (3.3.32)$$

in which $\alpha$ represents all the roots of equation $\overline{v}_0 + \overline{v}_1 \alpha + \overline{v}_2 \alpha^2 + \overline{v}_3 \alpha^3 + \overline{v}_4 \alpha^4 + \overline{v}_5 \alpha^5 = 0$. Based on the Fourier series theory, the dimensionless deflection $\phi (m, \tau)$ can therefore be derived as follows:

$$\begin{aligned}\phi(\zeta,\tau) &= 2\sum_{m=1,3,..}\phi_m(m,\tau)\,sin(r_m\zeta)\\ &= 96F_0\sum_{m=1,3,..}\frac{1}{r_m^5}\sum_{\alpha}\left(\frac{v_0+v_1\alpha+v_2\alpha^2+v_3\alpha^3+v_4\alpha^4}{\overline{v}_1+2\overline{v}_2\alpha+3\overline{v}_3\alpha^2+4\overline{v}_4\alpha^3+5\overline{v}_5\alpha^4}\right)e^{\alpha\tau}sin(r_m\zeta)\end{aligned} \tag{3.3.33}$$

Similarly, the dimensionless temperature $\theta_1(\zeta,\tau)$ can be derived as follows:

$$\theta_1(\zeta,\tau) = 96F_0\sum_{m=1,3,..}\frac{1}{r_m^5}\sum_{\alpha}\left(\frac{\widetilde{v}_1\alpha+\widetilde{v}_2\alpha^2}{\overline{v}_1+2\overline{v}_2\alpha+3\overline{v}_3\alpha^2+4\overline{v}_4\alpha^3+5\overline{v}_5\alpha^4}\right)e^{\alpha\tau}sin(r_m\zeta) \tag{3.3.34}$$

where $\widetilde{v}_1 = S_6(S_1+S_2r_m^2)\,r_m^4$, $\widetilde{v}_2 = \tau_1 S_6(S_1+S_2r_m^2)\,r_m^4$.

Eqs. (3.3.33) and (3.3.34) are the desired solution for deflection and temperature distribution along the thickness direction of the nanobeam considering nonlocal and MGT theories taking surface effects into account. The small-scale and surface effects on the vibration responses of deflection and temperature over time are thoroughly examined in the next section.

### 3.3.4 Numerical results and discussion

This section aims at deriving the simulated results obtained for a silicon nanobeam using the nonlocal elasticity theory and Moore-Gibson-Thompson (MGT) thermoelasticity theory under the influence of surface energy effects. For this, we carry out computational work on the basis of the theoretical results obtained in previous section. By splitting this part into four subsections, the effects of nonlocal parameter, surface energy, aspect ratios, and phase-lag time on dimensionless deflection and dimensionless temperature distribution along the thickness direction of the nanobeam with respect to dimensionless time are examined in depth. The behaviors of the deflection and tem-

perature fields have been found to converge to a steady state. The present results are compared to the earlier analytical results reported by Sun et al. (2006) as special cases. The properties of the Silicon nanobeam at reference temperature $T_0 = 293\,K$ are listed below (Sun et al., 2006):

$E = 169\,GPa$, $\rho = 2330\,kg/m^3$,$C_v = 713\,J/kgK$, $\alpha_T = 2.59 \times 10^{-6} K^{-1}$,$v = 0.22$, $k = 156\,W/mK$, $k^* = 156\,W/mKs$.

The surface tension $\sigma^0$ of certain materials, such as Silicon and GaAs, is typically around $0.1 - 1$ N/m, whereas the surface elastic modulus ($E^s$) is often around $1 - 10$ N/m (Miller and Shenoy, 2000; Wu and Dzenis, 2006). So, throughout the present study, the values of these parameters are set to be $\sigma^0 = 0.5$ N/m and $E^s = 5$ N/m except where the influences of these parameters are analyzed. Also, the value of phase-lag time $\tau_q$ in its dimensionless form $\tau_1$ is set to $\tau_1 = 0.1$ except where the impact of phase-lag time is shown. Additionally, the dimension of the nanobeam is considered as $L/h = 10$, $b/h = 0.5$, $h/h_0 = 0.5$ in which $h_0 = 20\,nm$ excluding those graphs where these effects are demonstrated. The vibration responses of dimensionless deflection and dimensionless temperature are shown in the dimensionless time range of $\tau = 0 - 100$. Additionally, the magnitude of uniform load $F$ is set to $F_0 = 1$, and the results are shown for first vibrational mode i.e., $m = 1$.

Figures 3.3.2($a$) and 3.3.2($b$) respectively illustrate the responses of deflection and temperature versus time without surface effect ($\sigma^0 = 0$, $E^s = 0$) under the classical theory ($\Omega = 0$) and the nonlocal elasticity theory ($\Omega \neq 0$) in the context of MGT thermoelasticity. The vibrations are in a quasi-steady state mode, as can be observed in the Figures. Sun et al. (2006) have also reported this fact for thermoelasticity theory with one relaxation parameter. The vibration amplitudes of deflection and temperature are clearly lower under nonlocal elasticity theory than under classical theory, which causes the energy to increase with time. The phase difference also increases with time when the nonlocal elasticity theory is applied.

Figures 3.3.3($a$) and 3.3.3($b$) depict the surface effects on the vibration of deflection and temperature versus time under nonlocal elasticity theory and MGT theory. From the Figures, it is clear that by considering the surface energy effects in the nanobeam, the energy dissipation of vibration can be reduced. Also, the surface effects become more pronounced as time increases. Thus, surface energy has a considerable influence on the vibration responses of deflection as well as on temperature of nanobeam.

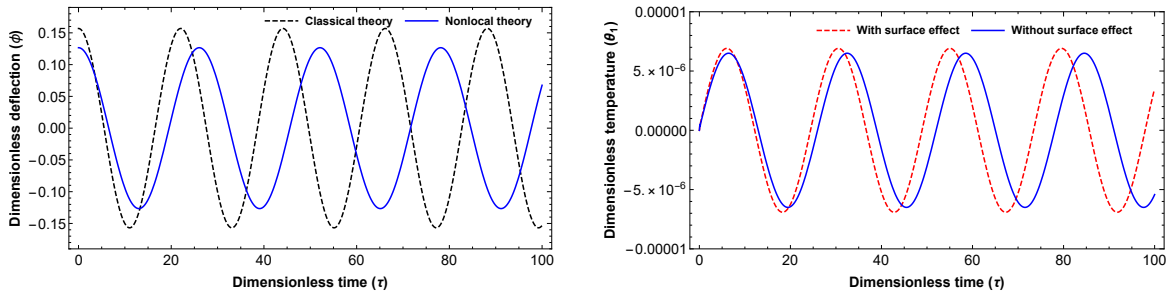


Figure 3.3.2: Responses of deflection and temperature versus time.

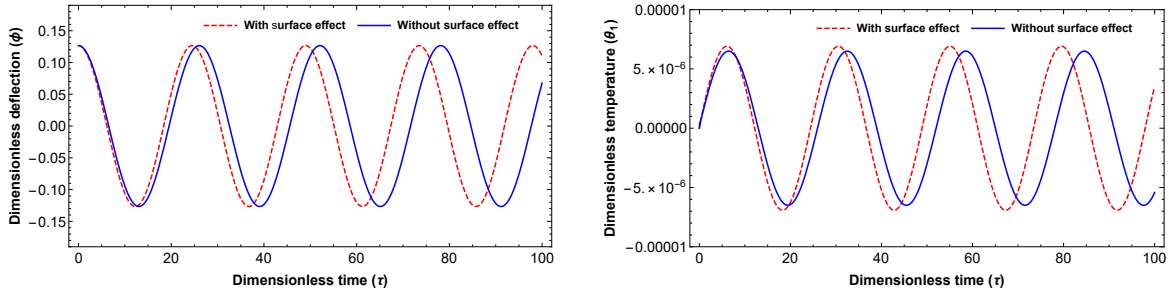


Figure 3.3.3: Responses of deflection and temperature versus time.

### 3.3.4.1 Small-scale effects

Figs. 3.3.4($a$) and 3.3.4($b$) respectively are presented to show the small-scale effects on the time-dependent deflection and temperature of the nanobeam for various values of

nonlocal parameter $\Omega$ (*i.e.*, $\Omega = 0,\ 0.2,\ 0.5,\ 0.8$). It can be observed in Fig. 3.3.4($a$) that the vibration response of deflection under classical theory ($\Omega = 0$) perfectly matches with the Fig. 1 in the Ref. (Sun et al., 2006). It is further demonstrated that there is a strong influence of nonlocal parameter on behavior of deflection and temperature of nanobeam. The amplitudes of deflection and temperature decrease with the increase in the values of nonlocal parameter. Thus, the maximum values of deflection and temperature are decreased, when the value of $\Omega$ is increased. It can also be observed from the results as displayed in Figs 3.3.4($a, b$) that the phase difference of the vibration increases with time as $\Omega$ approaches the maximum value. Hence, it is concluded that the variation in small-scale parameter $\Omega$ influences the elastic and temperature fields at nanoscale in the context of coupled generalized MGT thermoelasticity theory.

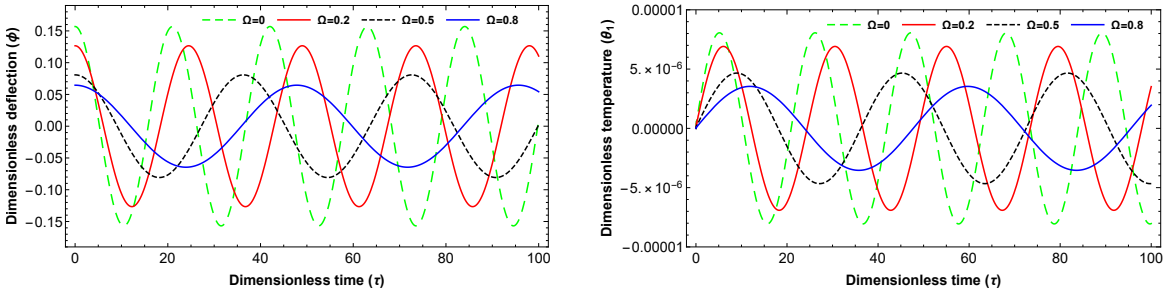


Figure 3.3.4: Effects of nonlocal parameter on deflection and temperature versus time.

### 3.3.4.2 Surface energy effects

In this subsection, the surface effects on deflection and temperature distribution along the thickness direction of the nanobeam versus time are investigated in depth for varying values of surface tension $\sigma^0$ (i.e., $\sigma^0 = 0.3$ N/m, 0.5 N/m, 0.8 N/m) and surface elastic modulus $E^s$ (i.e., $E^s = 3$ N/m, 5 N/m, 8 N/m) separately. Figures 3.3.5($a$) and 3.3.5($b$) depict the surface effects on nanobeam deflection versus time. It can be deduced from Fig. 3.3.5($a$) that when the value of surface tension increases, the vibration response

of the deflection gets quicker, resulting in the reasons of oscillation reduction. It is also found that the influence of surface tension is insignificant for short time intervals but considerable for longer time intervals. Figure 3.3.5($b$) shows the impact of surface elastic modulus $E^s$ on deflection with time. The variation in value of $E^s$ doesn't create any significant effect in the distribution diagrams of dimensionless deflection for short time range. However, as dimensionless time increases, the influence of $E^s$ on deflection becomes more significant, as seen in Figure 3.3.5($b$). Based on Figures 3.3.5($a$) and 3.3.5($b$), it is determined that the influence of surface tension $\sigma^0$ on deflection is greater than the influence of surface elastic modulus $E^s$.

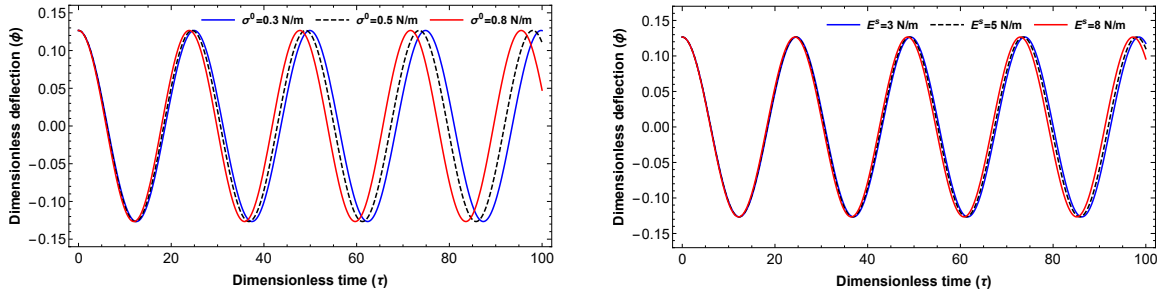


Figure 3.3.5: Effects of surface residual tension and surface elastic modulus on deflection versus time.

To see the influences of surface effects on dimensionless temperature of nanobeam versus dimensionless time, the impacts of surface tension $\sigma^0$ and surface elastic modulus $E^s$ on temperature are shown in Figs. 3.3.6($a$) and 3.3.6($b$), respectively. It is clear that at any time, the amplitude response of temperature of the nanobeam increases and peak values are attained much earlier by increasing the value of $\sigma^0$. It is further observed that the temperature response of nanobeam is not much affected by the variation of $E^s$ for smaller time range as displayed in Fig. 3.3.6($b$), whereas the effect is considerably pronounced at longer time. However, it is concluded from Figures 3.3.5 and 3.3.6 that the vibration responses of deflection and temperature are more affected by surface

tension ($\sigma^0$ ) as compared to surface elastic modulus ($E^s$).

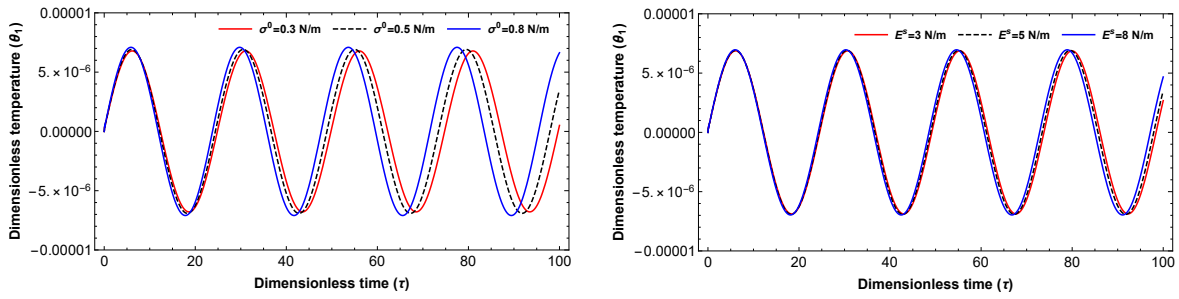


Figure 3.3.6: Effects of surface residual tension and surface elastic modulus on temperature versus time.

#### 3.3.4.3 Effects of aspect ratios of the nanobeam

This subsection focuses on the analysis of size effects of the nanobeam under nonlocal elasticity theory on the time history responses of deflection and temperature. Figs. 3.3.7($a$) and 3.3.7($b$) show the impacts of aspect ratios $L/h$ and $h/h_0$ of the nanobeam on the vibration response of deflection in the time range $\tau = 0 - 100$, respectively. It is found that the vibration response of deflection becomes faster when the length of the nanobeam is increased as shown in Fig. 3.3.7($a$). This implies that when the length of the nanobeam gets larger, the energy dissipation becomes smaller. Fig. 3.3.7($b$) indicates that when the thickness of the nanobeam reaches its characteristic thickness, the attenuation becomes stronger. Therefore, it may be concluded that when the thickness of the nanobeam is larger than its characteristic size, the effect of vibration weakens as the beam thickness increases. Thus, the vibration response of deflection may be increased for longer time by increasing the length and thickness of the nanobeam.

The effects of aspect ratios $L/h$ and $h/h_0$ on the time-dependent temperature of the nanobeam are displayed in Figs. 3.3.8($a$) and 3.3.8($b$), respectively. The time-dependent vibration responses of nanobeam's deflection and temperature are observed

to be affected by the size of the nanobeam significantly. It is demonstrated from the Figures that the temperature amplitudes get its maximum for smaller value of aspect ratio $L/h$, whereas for larger value of aspect ratio $h/h_0$. It is further observed that the effects of aspect ratios of the nanobeam's dimension on its temperature are more significant than its deflection as can be seen from Figs. 3.3.7 and 3.3.8.

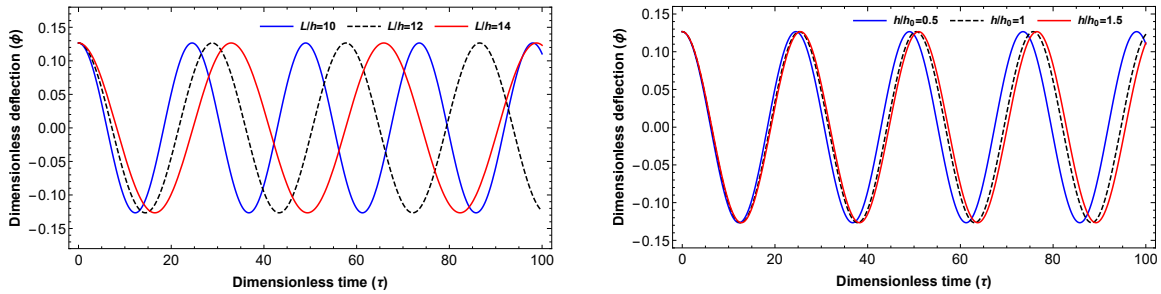


Figure 3.3.7: Effects of aspect ratios on deflection versus time.

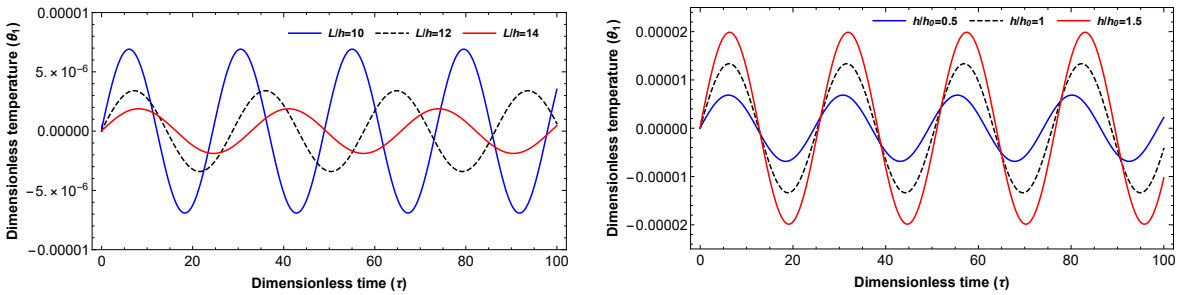


Figure 3.3.8: Effects of aspect ratios on temperature versus time.

### 3.3.4.4 Influence of phase-lag time

Based on nonlocal elasticity theory, this subsection depicts the effect of phase-lag times appeared in MGT thermoelasticity theory on vibration responses of deflection and temperature of the nanobeam. The results for varying the phase-lag time are shown

for $\tau_1 = 0$ (GN-III thermoelasticity theory), $\tau_1 = 0.5$, and $\tau_1 = 0.8$. According to Fig. 3.3.9($a$), changing the phase-lag time has no influence on the vibration response of the nanobeam's deflection over time. Hence, under nonlocal elasticity theory, the vibration response of deflection over time for GN-III and MGT thermoelasticity theories is nearly the same. In contrast, Fig. 3.3.9($b$) demonstrates that the modification of phase-lag time has a considerable effect on the vibration response of time-dependent temperature. Here, the temperature amplitude is noted to be higher under MGT theory as compared to GN-III theory. Moreover, the temperature attenuation under MGT theory exhibits the jumps in the starting during the time range $\tau = 0 - 10$ before it reaches its quasi-steady state mode of vibration quickly beyond time $\tau = 10$ as shown clearly from Figures 3.3.9($b, c$). Figure 3.3.9($c$) further indicates that increasing the value of phase-lag time increases the oscillation in temperature amplitude at the beginning over time. It is concluded that the temperature response becomes stronger as the phase-lag time increases, resulting in an increase in energy dissipation over time.

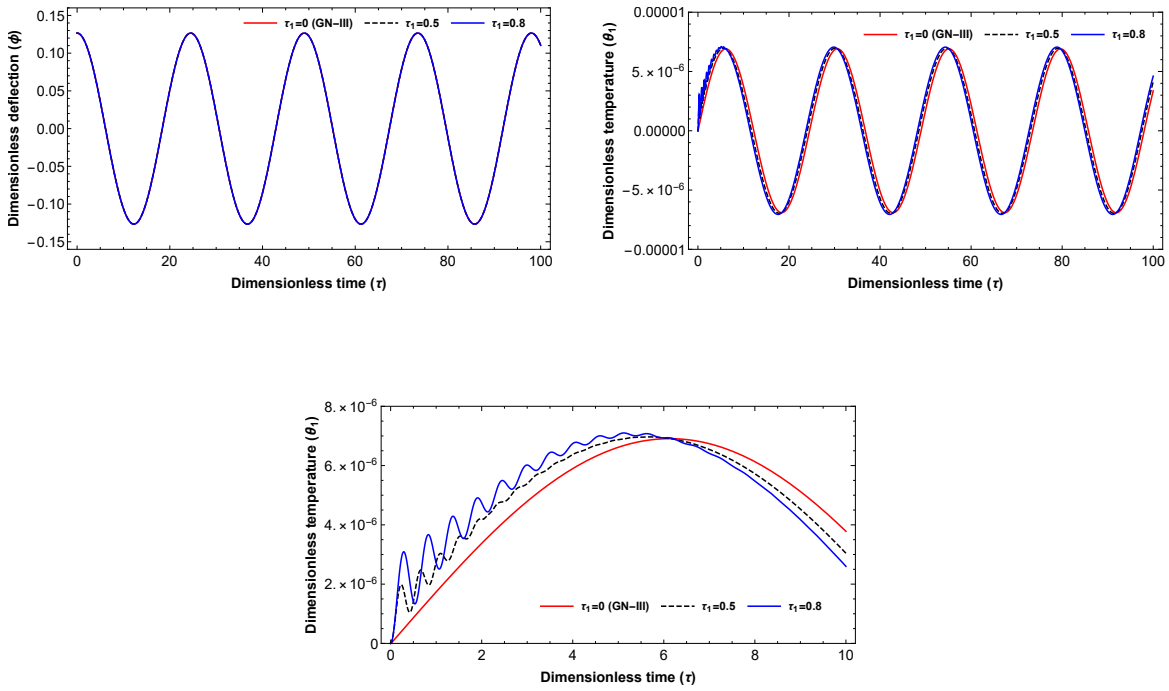


Figure 3.3.9: Effects of phase-lag time on deflection and temperature versus time.

### 3.3.5 Conclusion

The deflection and temperature responses of Silicon nanobeams are explored in this study using nonlocal elasticity and MGT thermoelasticity theories by taking surface effects into consideration. The surface effects due to the curvature generated by the bending of the nanobeam are considered. To get the solution for deflection and temperature distribution in the thickness direction of the nanobeam, the coupled governing equations are solved using the finite Fourier sine transform and Laplace transform techniques. The impacts of small-scale parameter, phase-lag time, length, thickness, and surface of the nanobeam on the vibration responses of deflection and temperature over time are thoroughly investigated. The following conclusions are made as the most highlighted findings:

- The vibration amplitudes of deflection and temperature over time are lower under the nonlocal elasticity theory than under the classical theory, which causes the energy dissipation to decrease with time.

- The amplitudes of deflection and temperature decrease significantly over time with the increase in the values of small-scale parameter.

- The influences of surface residual tension and surface elastic modulus on deflection and temperature responses are insignificant for short time intervals during vibration but it is considerable for longer time intervals. Furthermore, the surface residual tension creates significant effect on the vibration responses of deflection and temperature than surface elastic modulus.

- The time-dependent vibration responses of nanobeam's deflection and temperature are affected by the size of the nanobeam significantly.

- The variation in the value of phase-lag time has no influence on the vibration response of the nanobeam's deflection with respect to time, whereas a considerable effect has been observed on the temperature response over time.

This work emphasizes the advantages of nonlocal elasticity theory over classical theory considering MGT thermoelasticity theory at nanoscale structures. Also, the surface and size effects are shown to play an important role in the design of high-performance nanomechanical systems. Therefore, it is expected that this work will be useful in understanding the dynamic and mechanical behaviors of nanomechanical systems when small-scale and surface effects are taken into account.